DESIGN AND DEVELOPMENT OF GROUP-III NITRIDE BASED LEDS FOR UV-BLUE REGION FOR UNDERWATER COMMUNICATION

Dissertation submitted to

Visvesvaraya National Institute of Technology, Nagpur in partial fulfillment of the requirements for the award of the degree

Master of Technology

in

VLSI DESIGN

by

NAVEEN KUMAR MODUGU

(MT23MVD010)

Under the guidance of

Dr. Nikhil Deep Gupta

Center for VLSI and Nanotechnology
Visvesvaraya National Institute of
Technology Nagpur 440 010 (India)

June 2025

DESIGN AND DEVELOPMENT OF GROUP-III NITRIDE BASED LEDS FOR UV-BLUE REGION FOR UNDERWATER COMMUNICATION

Dissertation submitted to

Visvesvaraya National Institute of Technology, Nagpur in partial fulfillment of the requirements for the award of the degree

Master of Technology

in

VLSI DESIGN

by

NAVEEN KUMAR MODUGU

(MT23MVD010)

Under the guidance of

Dr. Nikhil Deep Gupta

Center for VLSI and Nanotechnology
Visvesvaraya National Institute of Technology Nagpur 440 010 (India)

June 2025

©Visvesvaraya National Institute of Technology, Nagpur 2025

Center for VLSI and Nanotechnology

Visvesvaraya National Institute of Technology, Nagpur

DECLARATION

I, **NAVEEN KUMAR MODUGU**, hereby declare that this dissertation titled, "**DESIGN AND DEVELOPMENT OF GROUP-III NITRIDE BASED LEDS FOR UV-BLUE REGION FOR UNDERWATER COMMUNICATION**" is carried out by me in the Department of **Center for VLSI and Nanotechnology** of Visvesvaraya National Institute of Technology, Nagpur. The work is original and has not been submitted earlier whole or in part for the award of any degree/diploma at this or any other Institution / University.

Naveen Kumar Modugu
Date:

Certificate

This to certify that the dissertation titled "**Design and Development of Group-III nitride based LEDs for UV-Blue region for underwater communication**" is submitted by **Naveen Kumar Modugu** in partial fulfillment of the requirements for the award of the degree of **Master of Technology in VLSI Design**, VNIT Nagpur. The work is comprehensive, complete and fit for final evaluation.

Dr. Nikhil Deep Gupta
Centre for VLSI and Nanotechnology
VNIT, Nagpur.

Prof. S. B. Dhok
Head, Center for VLSI and Technology
VNIT, Nagpur
Date:_____

Center for VLSI and Nanotechnology
Visvesvaraya National Institute of Technology, Nagpur

June 2025

Date: _____

Non-Plagiarism Certificate

Certified that M. Tech Dissertation titled **"DESIGN AND DEVELOPMENT OF GROUP-III NITRIDE BASED LEDS FOR UV-BLUE REGION FOR UNDERWATER COMMUNICATION"** submitted by **Naveen Kumar Modugu (MT23MVD010)** has been checked for plagiarism using TURNITIN software and the overlap is found within prescribed limits. A summary of the report is given below:

Naveen Kumar Modugu

Date:

Dr. Nikhil Deep Gupta

Assistant Professor

Acknowledgement

I would like to express my heartfelt gratitude to my project supervisor, **Dr. Nikhil Deep Gupta**, Assistant Professor at the Center of VLSI and Nanotechnology at Visvesvaraya National Institute of Technology (VNIT) in Nagpur, for his invaluable guidance, constant encouragement, and expert supervision throughout the project. His insightful suggestions and technical inputs were instrumental in shaping this work.

I am deeply thankful to **Prof. R. M. Patrikar, Prof. R. B. Deshmukh, Prof. S. B. Dhok, Dr. G. C. Patil, and Dr. Vasu Pulijala** for their continuous support, motivation, and the academic environment they have fostered at VNIT, which has been immensely beneficial to my learning and development. I also extend my sincere thanks to the Director, VNIT Nagpur, for providing the necessary infrastructure, research facilities, and institutional support during this project.

I would like to acknowledge the unwavering support of my friends, family and juniors who have stood by me during challenging times and offered their guidance, strength, and inspiration. Their emotional support and encouragement helped me remain focused and motivated.

Finally, I would like to thank all my fellow students and colleagues whose collaboration, discussions, and insights enriched my academic journey. Their camaraderie and shared enthusiasm made this endeavor both fruitful and memorable.

Naveen Kumar Modugu

ABSTRACT

In an era driven by smart technology and high-speed data exchange, the demand for efficient, compact, and reliable optical communication systems has skyrocketed—especially for challenging environments like underwater. This project dives into the design and simulation of light-emitting diodes (LEDs) using Group-III nitride semiconductors, focusing on the UV-blue region of the spectrum, which offers lower absorption and better propagation in aquatic mediums. By engineering multiple quantum well (MQW) structures based on InGaN/GaN heterojunctions, we tailored the emission wavelength through careful indium composition tuning. Using TCAD Sentaurus simulations, we analyzed optical and electrical behaviors, modeled carrier dynamics, and optimized layer parameters for enhanced performance. Special attention was given to mitigating internal electric field effects—like spontaneous and piezoelectric polarization—by exploring different crystal orientations and employing electron-blocking layers.

The proposed structure utilizes an InGaN/GaN multi-quantum well (MQW) heterostructure grown on a GaN substrate. By carefully tuning the indium content and optimizing quantum well and barrier thickness, the device achieves precise bandgap control to generate UV-blue light. To overcome internal electric field limitations caused by spontaneous and piezoelectric polarization in the c-plane GaN, advanced strategies like electron blocking layers (EBLs) and crystal orientation tuning were incorporated. Using Synopsys Sentaurus TCAD, detailed simulations were carried out to study carrier distributions, radiative recombination rates, and optical output efficiency under different conditions, including variations in aluminum composition in the EBL. The results confirm that the optimized structure ensures strong carrier confinement, high internal quantum efficiency, and reduced efficiency droop.

The final LED structure shows promise for underwater optical communication, offering efficient photon emission in the 370–410 nm range. With further advancements, these GaN-based devices can pave the way for compact, high-speed, and low-power underwater communication networks.

List of Figures

1.1 Single Quantum Well heterostructure LED……..6

2.1 Insulators' Band diagrams 2) Semiconductors 3) Metals……..10

2.2 An E-K diagram showing semiconductors with direct and indirect band gaps…….…….12

2.3 Tunable group-III-nitride ternary alloy bandgaps. Energy BG versus lattice constant (parameter) of group III-V semiconductors……..13

2.4 Wurtzite crystal structure of GaN with different polarities (Ga- Faced and N-Faced) …….14

2.5 (a) Hexagonal Unit Cell (b) Atomic structure of Ga- and N-polar GaN……..16

2.6 Representation of polar, Non-polar, and Semi-polar GaN substrates…….18

2.7 Sentaurus Workbench Tool……..24

3.1 Effective mass of electron and hole of $In_xGa_{(1-x)}N$ for mole fraction x…….37

3.2 CRI of $In_{0.05}Ga_{0.95}N$ vs Wavelength (nm)…….. 38

3.3 CRI of $In_{0.1}Ga_{0.9}N$ vs Wavelength (nm)…….. 38

3.4 CRI of $In_{0.2}Ga_{0.8}N$ vs Wavelength (nm)…….. 39

3.5 Shows the Polarization along the c-axis……..40

4.1 LED structure used for modeling……..43

4.2 Multiple Quantum Wells LED……....44

4.3 Developed 3D LED…….46

5.1 Band Diagram…….47

5.2 Distribution of electrons from p-GaN to n-GaN along the LED……..…..48

5.3 Distribution of holes from p-GaN to n-GaN along the LED……...…49

5.4 Electron distribution rate in the LED with different amounts of Al……..…...50

5.5 Hole distribution rate in the LED with different amounts of Al……..….51

5.6 Rates of radiative recombination in the LED with different Al composition….52

5.7 I-V curve……53

List of Tables

2.1 Lattice Parameters of GaN……...16

2.2 Basic properties of III-Nitride Wurtzite structure……....19

2.3 Energy Bandgap (eV) of $In_xGa_{1-x}N$ at mole fraction x……..22

3.1 $In_xGa_{1-x}N$ alloys absorption coefficient computation using fitting parameters….36

3.2 Effective mass of electron and hole of $In_xGa_{(1-x)}N$ w.r.t change in mole fraction x……...36

Abbreviations

TMM-Transfer Matrix Method

CRI-Complex Refractive Index

SRH-Shockley-Read-Hall

QCSE-Quantum Confined Stark Effect

EQE- External Quantum Efficiency

IQE-Internal Quantum Efficiency

EBL-Electron Blocking Layer

Table of Contents

Abstract ..... **i**

List of Figures ..... **ii**

List of Tables ..... **iv**

Abbreviations ..... **v**

Chapter1: - Introduction **1**

1.1 Introduction 2

1.2 Working of LED 2

1.3 Milestones in GaN Doping and p-type Conductivity 4

1.4 Emergence of InGaN and Bandgap Engineering 5

1.5 Evolution from Double to Multi-Quantum Well Structures 6

Chapter 2: - Recent Advancements in Group III-Nitrides and Methodology **8**

2.1 Semiconductor Physics 9

2.2 Energy–Momentum (E–k) Diagram and Band Structure 10

2.3 Group III-Nitrides (III–V Elements) 12

2.4 Gallium Nitride (GaN) 13

2.4.1 Polar GaN 15

2.4.2 Non-Polar GaN 17

2.4.3 Semi-Polar GaN 17

2.5 Indium Nitride (InN) 20

2.5.1 Indium Gallium Nitride (InGaN) 20

2.6 Bandgap Energy of InGaN 20

2.7 Synopsys Sentaurus TCAD 22

2.7.1 Sentaurus Tool Flow 22

2.7.2 Sentaurus Structure Editor (SDE) 24

2.7.3 Sentaurus Device (SD) 25

2.8 Quantum Well 26

2.9 Light Emitting Diode 27

2.9.1 Carrier Generation in LEDs 28

2.9.2 Recombination Mechanisms 29

2.9.2.1 Radiative Recombination 29

2.9.2.2 Shockley–Read–Hall (SRH) Recombination 29

2.9.2.3 Auger Recombination 30

2.10 Ray Tracing 30

Chapter 3: - Calculation of optical properties of III-V Nitrides 32

3.1 Introduction 33

3.2 Complex refractive Index of InxGa1-xN 33

3.3 Polarization Effects in Group III-Nitride Heterostructures 39

Chapter 4: - Proposed Structure Design……42

4.1 Introduction 43

4.2 Device Configuration 43

4.3 Structural Design and Fabrication Considerations 44

4.4 Final Optimized parameters 45

Chapter 5: - Results and Discussion 46

5.1 Band Diagram 47

5.2 Distribution of electron and hole from p-GaN to n-GaN along the LED in Presence

and Absence of AlGaN EBL…….....47

5.3 Rates of radiative recombination, electron-distribution and hole-distribution in the LED with different Al composition in AlGaN EBL……...49

5.4 LEDCharacterization……..……... 55

5.4.1 Electrical Characterization (I-V Analysis)……. 55

5.4.2 Carrier Distribution……..…… 55

5.4.3 Radiative Recombination Rate……...…… 55

Chapter 6: - Conclusion and Future Work…….57

References Work……58

1

INTRODUCTION

Chapter 1: Introduction

1.1 Introduction

Thomas Edison created the incandescent lightbulb in 1879 marked a pivotal moment in the evolution of artificial lighting. Since then, the demand for lighting technologies that are not only cost-effective but also more efficient and durable has continued to grow. Over the decades, various lighting solutions such as filament-based lamps for household use, fluorescent lights for commercial environments, and sodium-vapor lamps for street illumination have been developed to meet this demand.However, these traditional light sources come with significant limitations, particularly in terms of energy efficiency and operational lifespan. This has led to the emergence and rapid advancement of solid-state lighting technologies, most notably light-emitting diodes (LEDs). LEDs have transformed the lighting industry due to their superior performance, long operational life, and adaptability across a wide range of applications. One notable example of the innovative use of LEDs is NASA's WARP 75 system, which comprises an array of LEDs used to support plant growth in space environments. Research has shown that exposure to near-infrared LED light can significantly accelerate cellular activity—up to 150 to 200 times faster than in untreated cells. This remarkable property has extended the use of such LED systems beyond space applications into medical therapies, such as improving the recovery process in bone marrow transplant patients.

The versatility and efficiency of LEDs have also found a place in the automotive sector. The introduction of full LED headlight systems by manufacturers like Audi represents a major shift in vehicle lighting technology, promising enhanced visibility, aesthetic appeal, and energy savings.Central to all these advancements is the continued effort to design and develop high-performance, energy-efficient LEDs that can meet the growing demands of modern technology and society.

1.2 Working of LED

LEDs are precisely designed semiconductor p-n junctions that emit light and function as transducers, converting electrical energy into light through a mechanism known as electroluminescence. When a forward bias is applied, electrons and holes recombine across the junction, releasing energy in the form of photons. The color—or wavelength—of the

emitted light is primarily governed by the bandgap energy of the semiconductor material. This relationship can be expressed by the formula:

$$\text{Energy of the photon that was released, } E = \frac{hc}{\lambda} \quad (1.1)$$

where h is Planck's constant, c is the speed of light, and λ is the wavelength of the emitted photon.

The development of LED technology traces back to the 1920s, with early devices made from silicon carbide (SiC). However, these early LEDs were extremely inefficient, achieving light emission efficiencies of less than 0.005%, which spurred interest in exploring alternative materials. Significant progress came in 1954 with the advent of III-V compound semiconductor LEDs, marking a new era for optoelectronic devices. These materials, such as gallium arsenide (GaAs), were attractive due to their direct wide bandgaps, making them suitable for efficient light emission. In 1962, research RCA, GE, IBM, and MIT groups independently reported infrared-emitting GaAs-based LEDs, achieving efficiencies in the range of 0.2% to 0.35%.The first visible-spectrum LEDs emerged through alloying techniques, particularly using gallium arsenide phosphide (GaAsP). By tuning the composition of GaAs and GaP, red, orange, and green emissions became possible. However, efficiency remained a significant challenge. For instance, pure GaAs LEDs had efficiencies around 0.2%, but introducing 44% phosphorus led to a dramatic drop in output efficiency, falling below 0.005%.

In recent years, AlInGaP-based materials have become increasingly significant for LED applications, particularly for emissions in the yellow-to-green spectrum. These devices typically exhibit a peak emission wavelength near 570 nm, accompanied by an external quantum efficiency (EQE) of approximately 1% [15]. However, attempts to push the emission wavelength further toward the green region have encountered a trade-off—efficiency tends to decline due to changes in the band structure. As the band structure of AlInGaP alloys transitions toward an indirect bandgap, photon emission becomes less efficient, thereby limiting their performance in the green spectral range.

The exploration of gallium nitride (GaN) as a potential material for visible LEDs dates back to the 1960s. A pivotal figure in this early research was James Tietjen, then Director

at the Radio Corporation of America (RCA). His team started looking into GaN. with the goal of achieving visible light emission. In 1969, Maruska and Tietjen successfully reported the growth of single-crystal GaN on sapphire substrates [16], marking a significant milestone in nitride semiconductor research.

The synthesis of GaN in their work involved the chemical reaction between liquid gallium and ammonia, as represented by the subsequent response:

$$2Ga + 2NH_3 \rightarrow 2GaN + 3H_2 \quad (1.2)$$

Inadvertently, GaN films were n-type, a common issue due to native defects or residual impurities. However, creating p-type GaN posed a substantial challenge. Early attempts involved doping GaN with zinc, but this resulted in an insulating behavior rather than the desired p-type conductivity. Despite this limitation, Pankove et al. were able to fabricate one of the first GaN-based LEDs using a structure that included an undoped n-type layer, a Zn-doped insulating region, and an indium surface contact [17]. The emission wavelength of this device varied across the visible spectrum-red, green, blue, or yellow-depending on the concentration of zinc.

1.3 Milestones in GaN Doping and p-type Conductivity

Progress continued in 1972 when Maruska and colleagues proposed the use of magnesium (Mg) as a dopant in place of zinc [18]. This led to the development of GaN LEDs that emitted light around 430 nm, a significant advancement toward efficient blue LEDs. Since then, magnesium has become the standard acceptor dopant for all commercially viable GaN-based LEDs. Nevertheless, achieving stable and conductive p-type GaN remained problematic due to passivation of Mg acceptors by hydrogen during the growth process. A major breakthrough occurred in 1989, when Amano et al. demonstrated that low-energy electron beam irradiation could activate the Mg dopants and dramatically enhance photoluminescence-by up to two orders of magnitude [19]. Subsequent work by Van Vechten et al. provided a theoretical explanation, suggesting that Mg forms a neutral Mg–H complex, which passivates its acceptor behavior and suppresses p-type conduction. The application of electron beam radiation breaks this complex, allowing magnesium to act as a shallow acceptor, typically about 0.16 eV above the valence band [20].

Gallium Nitride (GaN), with its wide direct band gap of approximately 3.4 eV, stands out as a highly versatile semiconductor material. When alloyed with other Group III-nitride compounds such as Indium Nitride (InN) and Aluminum Nitride (AlN), GaN can form a broad spectrum of ternary alloys like InGaN and AlGaN. These combinations enable precise band gap tuning, a process vital for adjusting the optical characteristics of the material to various optoelectronic applications, including light-emitting diodes (LEDs), laser diodes, and photodetectors.

1.4 Emergence of InGaN and Bandgap Engineering

A significant breakthrough in GaN-based optoelectronics occurred in 1995 when Shuji Nakamura of Nichia Corporation in Japan effectively demonstrated the first blue and green LEDs that were based on InGaN double heterostructures. This milestone was achieved through the technique of band gap engineering, wherein the composition of InN and GaN was carefully adjusted to tune the emission wavelength. By manipulating the indium content in the InGaN alloy, emissions across a wide spectral range—from approximately 1.0 eV (near-infrared) to 3.4 eV (ultraviolet)became achievable. The LEDs produced during this pioneering work achieved external quantum efficiencies of around 10%, marking a substantial leap forward in solid-state lighting technology. The success of these early devices laid the foundation for the modern GaN-based LED industry, which now powers a wide range of applications, from energy-efficient lighting to high-speed communication systems. The ability to fine-tune emission properties through quantum well design and alloy composition remains a core strength of III-nitride semiconductors.

$$x(GaN) + 1 - x(InN) \longrightarrow In_{1-x}Ga_xN \tag{1.3}$$

Because of the pioneering development of InGaN-based blue and green LEDs, ternary III-nitride compounds such as InGaN have emerged as the material of choice for active layers in quantum well structures. GaN-based optoelectronic devices typically incorporate combinations like GaN/AlGaN or GaN/InGaN to form quantum wells (QWs) that enable efficient light emission across a wide spectral range. The ability to engineer these heterostructures has been fundamental to the evolution of LED technology.

1.5 Evolution from Double to Multi-Quantum Well Structures

The growth of InGaN films is typically achieved using the two-flow Metal-Organic Chemical Vapor Deposition (MOCVD) technique. During this process, various precursors are used to supply the constituent elements: Trimethylgallium (TMG), Trimethylaluminum (TMAl), and Trimethylindium (TMI) serve as sources for Ga, Al, and In respectively. Additional dopants such as Si, Mg, and Zn are introduced using gases like monosilane (SiH_4), bis-cyclopentadienyl magnesium (Cp_2Mg), and diethylzinc (DEZ), with ammonia (NH_3) acting as the nitrogen source.

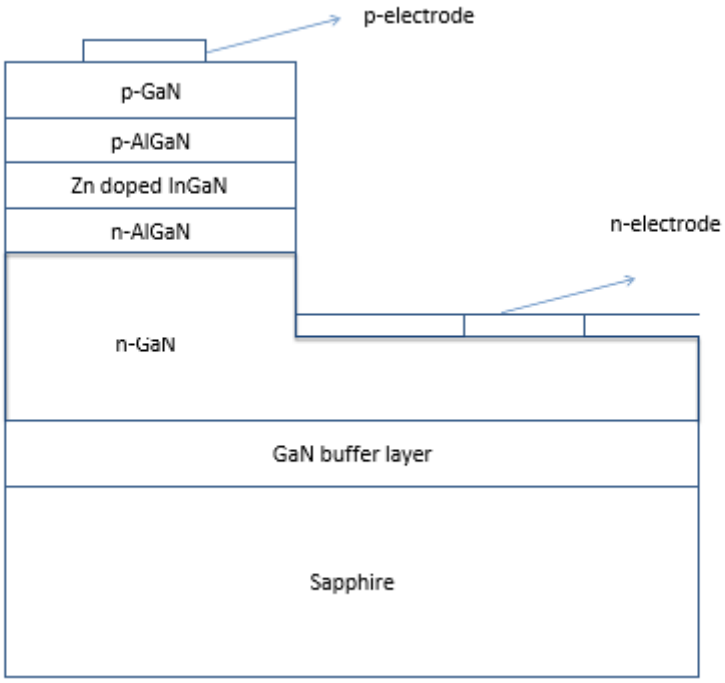

Figure 1.1: Single Quantum Well heterostructure LED [2].

As stated by Nakamura et al., MOCVD was used to grow every layer in the first double heterostructure LED, which is depicted in fig. 1.2. While the Ti/Al contact was evaporated to n-GaN after etching the p-GaN and the quantum wells, the Ni/Au layer was directly evaporated onto p-GaN to create the p-contact [2]. A 2.7% external efficiency has been achieved. using this LED.In the early InGaN-based double heterostructure LEDs developed by Nakamura and his team, all layers were deposited using MOCVD. The p-type contact was realized by directly evaporating a Ni/Au layer onto the p-GaN, while the n-type contact was formed by etching through the p-GaN and

quantum wells to deposit Ti/Al onto the n-GaN. These initial devices demonstrated an external quantum efficiency (EQE) of about 2.7%, marking a significant technological milestone.

Subsequent advancements focused on multi-quantum well (MQW) structures rather than bulk InGaN layers. These MQW devices provided a substantial improvement in optical efficiency—by almost two orders of magnitude—due to enhanced carrier confinement and reduced non-radiative recombination. As a result, Blue and green MQW LEDs' exterior quantum efficiency was reported to reach approximately 10% and 7%, respectively.

Despite these improvements, a major design challenge persists: how to maximize light output while minimizing input power and thermal losses. Achieving higher internal quantum efficiency (IQE) is largely dependent on the structural design and the quality of material growth, particularly the interface sharpness, well-barrier thickness control, and defect density.

Even with high IQE, many LEDs suffer from low external efficiency due to total internal reflection, which traps a significant portion of generated light within the device. Addressing this issue has led to numerous design strategies aimed at improving light extraction efficiency (LEE). These include surface texturing, photonic crystal structures, and the use of reflective layers—all of which will be discussed in later sections of this thesis.

2

RECENT ADVANCEMENTS IN GROUP - III NITRIDES AND METHODOLOGY

Chapter 2: Theory

2.1 Semiconductor Physics

The basic characteristics described in this chapter are of semiconducting materials, with a focus on the principles behind semiconductor devices, p-n junctions, and light-emitting diodes (LEDs) as a specific class of optoelectronic devices.

At the most basic level, materials can be broadly categorized into three groups: conductors, insulators, and semiconductors [26].

- Conductors are materials where atoms' outer (valence) electrons are freely bonded and have unrestricted mobility throughout the structure. This high mobility of electrons allows for excellent electrical conductivity. In such materials, the conduction and valence bands overlap, eliminating any significant energy barrier for electron flow. Metals, such as copper and aluminum, are classic examples of conductors.
- Insulators, on the other hand, possess tightly bound valence electrons that are not easily excited into the conduction band. These materials are characterized by a large energy gap (bandgap) between the valence and conduction bands, which prevents free movement of charge carriers under normal conditions. Examples include materials like glass, plastic, and rubber.
- Semiconductors exhibit electrical properties that fall between those of conductors and insulators. Their conductivity can be precisely tailored, making them essential for electronic and optoelectronic applications. Semiconductors may be classified into two main types:
    - Elemental semiconductors, such as silicon (Si) and germanium (Ge), are composed of single elements from Group IV of the periodic table.
    - Compound semiconductors, like gallium nitride (GaN) and gallium arsenide (GaAs), are formed by combining elements from Groups III and V. These materials are particularly significant for optoelectronic devices due to their direct bandgaps, which facilitate efficient light emission.

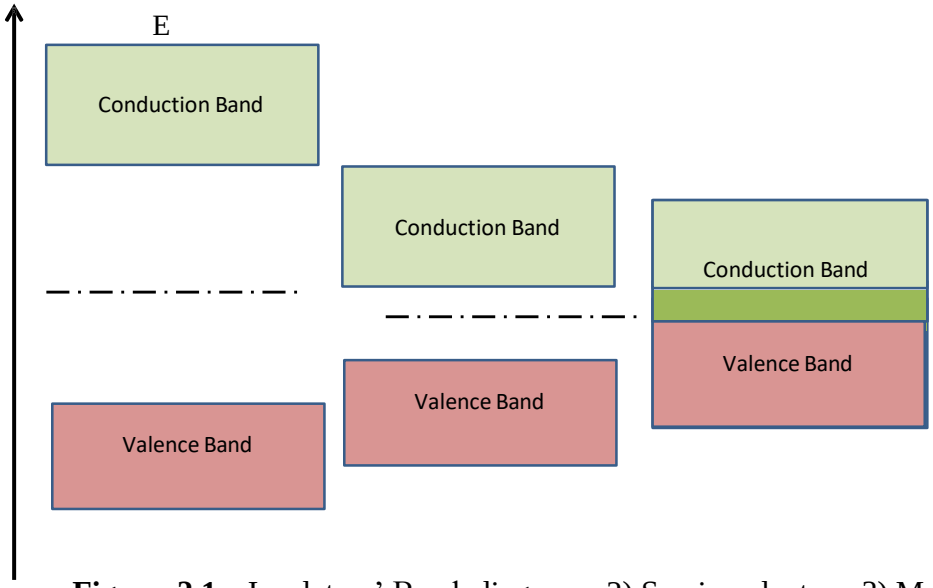

Figure 2.1: Insulators' Band diagrams 2) Semiconductors 3) Metals.

Dopants, or impurities, can be added to semiconductors to change their electrical characteristics. added in controlled amounts. A pure semiconductor is referred to as intrinsic, where charge carriers (electrons and holes) are generated solely by thermal excitation. When dopants are introduced, the material becomes extrinsic, and its conductivity is significantly enhanced.

- n-type semiconductors are formed by doping the material with atoms that have more valence electrons than the host atom (e.g., phosphorus in silicon), thereby introducing additional free electrons as charge carriers.
- p-type semiconductors result from doping with elements that have fewer valence electrons (e.g., boron in silicon), which creates holes—vacant sites in the atomic structure that behave like positive charge carriers.

The precise control of dopant type, concentration, and spatial distribution is critical in the fabrication of modern semiconductor devices. It forms the foundation for creating p-n junctions, the building blocks of diodes, transistors, and light-emitting devices.

2.2 Energy–Momentum (E–k) Diagram and Band Structure

Understanding the electronic properties of a material requires examining its energy-momentum (E–k) relationship, often represented through E–k diagrams. These plots play

a crucial role in characterizing key parameters such as the electron affinity, Fermi level, and band gap energy, each of which uniquely defines a material's behavior.

The band gap energy is the minimum energy difference between the top of the valence band and the bottom of the conduction band. In conductors, this gap is nearly zero, allowing free flow of electrons. Insulators have a wide band gap, preventing electron excitation at room temperature, while semiconductors fall in between, with a moderate gap that allows controlled conductivity.

The Fermi level represents the highest energy level occupied by electrons at absolute zero. It serves as a reference for understanding how electrons populate energy states within a material. On the other hand, electron affinity refers to The energy needed to release an electron from a solid's conduction band into a vacuum. These parameters collectively influence a material's band alignment and its performance in electronic and optoelectronic devices.

Semiconductors can be further categorized based on their band gap nature into:

- Direct band gap semiconductors: In these materials, the minimum of the conduction band and the maximum of the valence band occur at the same crystal momentum (k-vector). This alignment enables electrons in the conduction band to directly recombine with holes in the valence band, releasing energy in the form of light. This property makes direct band gap materials—like GaAs and GaN—highly suitable for light-emitting applications.
- Indirect band gap semiconductors: These materials, such as silicon and germanium, exhibit Valence band maxima and conduction band minima at various k-vectors. As a result, electron-hole recombination requires the involvement of a phonon (lattice vibration) to conserve momentum. This additional step reduces the efficiency of radiative recombination, making indirect semiconductors less suitable for LEDs and lasers.

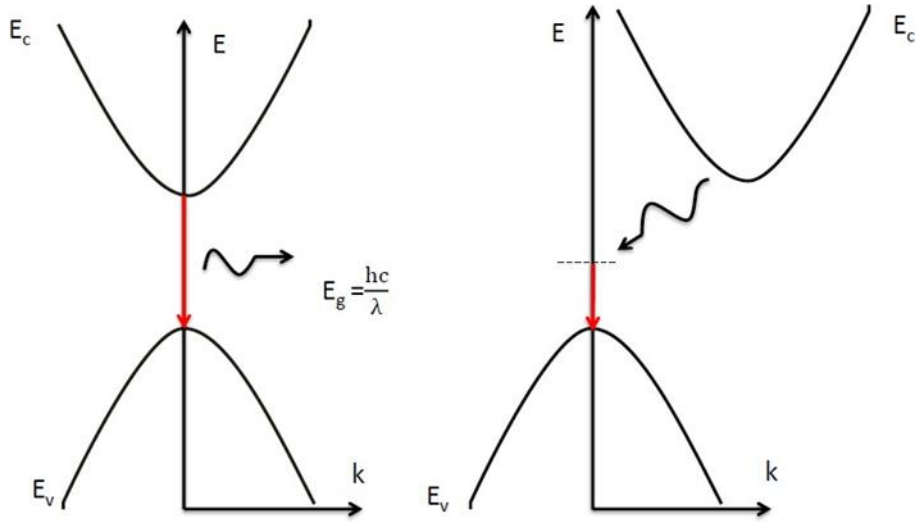

Figure 2.2: An E-K diagram showing semiconductors with direct and indirect band gaps[7]

2.3 Group III-Nitrides (III–V Elements)

Group III-nitride semiconductors, which include gallium nitride (GaN), indium nitride (InN), and aluminum nitride (AlN), are widely recognized for their wide and tunable band gaps, making them essential materials for advanced electronic and optoelectronic applications. These semiconductors offer excellent performance across a range of wavelengths and operating conditions.

At room temperature (approximately 300 K), the bandgap values for the individual nitrides are:

- InN: ~0.7 eV
- GaN: ~3.42 eV
- AlN: ~6.2 eV

This broad spectrum of bandgap energies allows for the engineering of ternary alloys such as InGaN and AlGaN, which enable tunable emission across the ultraviolet, visible, and infrared spectrums. The ability to tailor the bandgap by varying the composition of these alloys offers a significant advantage in designing devices like LEDs, laser diodes, and high-power transistors.

The crystal structure of group III-nitrides can appear in two primary forms:

- Wurtzite (hexagonal)
- Zinc blende (cubic)

Among these, the wurtzite phase is thermodynamically more stable under standard ambient conditions and is, therefore, the most commonly observed in naturally grown and commercially developed III-nitride materials.

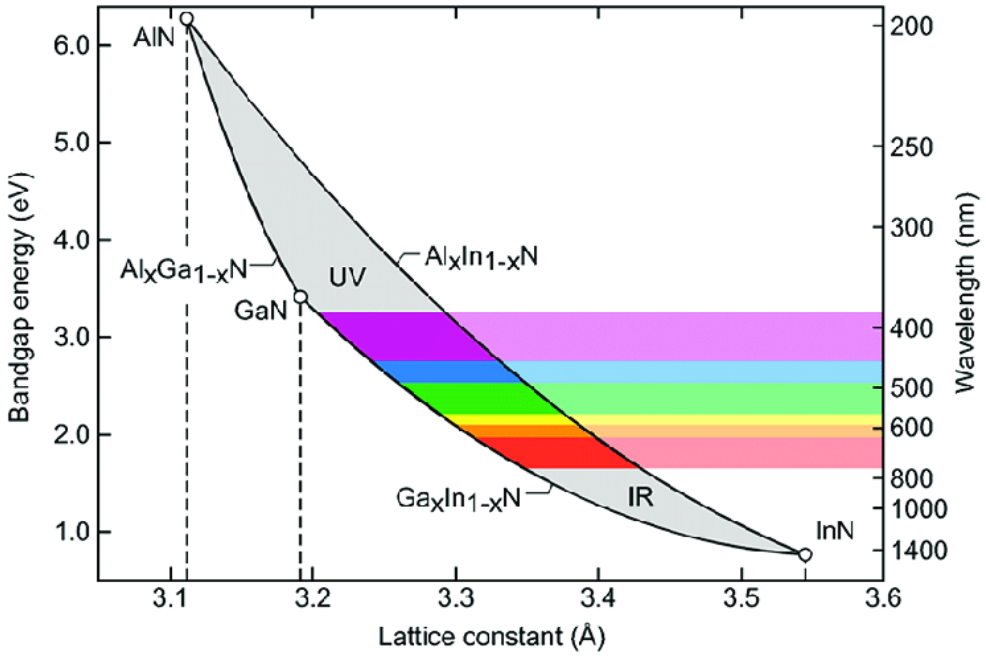

Fig 2.3 Tunable group-III-nitride ternary alloy bandgaps. Energy BG versus lattice constant (parameter) of group III-V semiconductors. (Tien Khee Ng). [9]

2.4 Gallium Nitride (GaN)

Gallium Nitride (GaN) is a compound semiconductor belonging to the group III–V family, known for its direct and wide bandgap properties. This material has emerged as a leading candidate for high-performance electronic and optoelectronic applications, thanks to its excellent physical and electrical characteristics.

Some of the most notable features of GaN include:

- High breakdown voltage
- Low on-resistance
- Fast switching speeds
- Superior thermal conductivity
- High power density and frequency capability

These advantages make GaN particularly suitable for high-power, high-frequency, and high-temperature applications, where traditional materials like silicon fall short. In fact, GaN has been shown to outperform silicon significantly in critical areas:

- It possesses a bandgap nearly three times wider than silicon (~3.41 eV compared to ~1.12 eV),
- Breakdown strength roughly 10 times higher, allowing operation under stronger electric fields,
- And carrier mobility that contributes to faster switching and reduced energy loss.

The wider bandgap also enables the design of transistors with shorter depletion widths and higher carrier concentrations, which are essential for compact and efficient device structures.

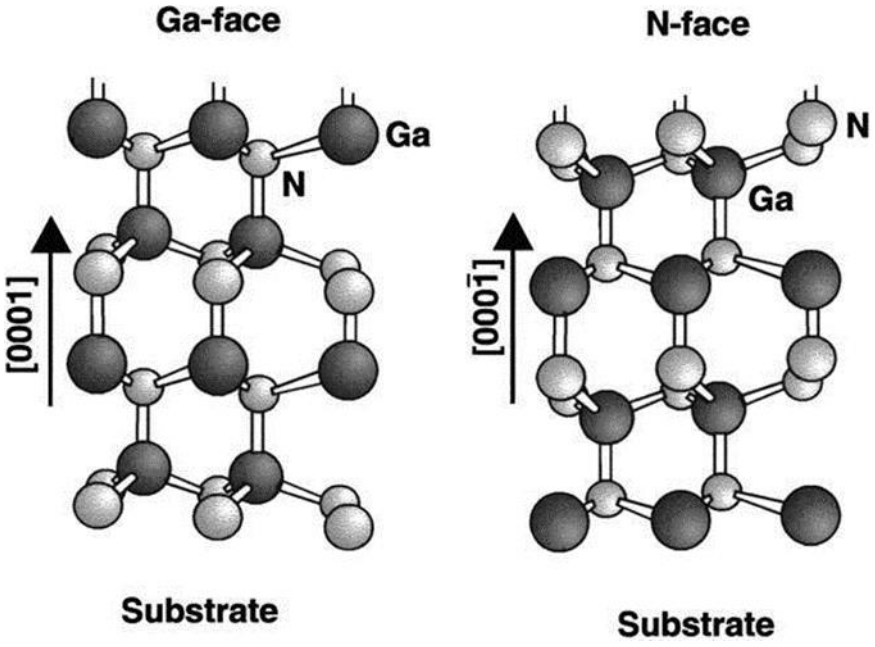

Fig 2.4 Wurtzite crystal structure of GaN with different polarities (Ga- Faced and N-Faced) [10]

Crystallographically, GaN can exist in both wurtzite (hexagonal) and zinc blende (cubic) forms. However, under standard growth conditions, the wurtzite structure is more stable and widely used. Both forms exhibit direct bandgap behavior**,** which is ideal for optoelectronic devices such as LEDs and laser diodes**.**

In terms of doping, silicon (Si) is typically used as the n-type dopant, while magnesium (Mg) serves as the most common p-type dopant. However, achieving high-quality p-type GaN remains challenging due to lower hole mobility and difficulties in activation of Mg. Moreover, the incorporation of dopants can induce strain and stress in the crystal lattice, influencing the material's microstructure and performance.

One of GaN's standout attributes is its chemical and thermal stability**.** The strong atomic bonding within the crystal makes it resistant to degradation under harsh environmental conditions**,** further enhancing its reliability in demanding power and RF (radio frequency) applications.

Based on its crystallographic structure, Gallium Nitride (GaN) can be classified into three distinct crystal orientations:

1. Polar GaN
2. Non-Polar GaN
3. Semi-Polar GaN

Each of these orientations plays a crucial role in influencing the physical, electrical, and optical properties of GaN-based devices. The orientation of the crystal affects parameters such as spontaneous and piezoelectric polarization, carrier recombination efficiency, and strain effects, which are particularly significant in optoelectronic applications like light-emitting diodes (LEDs) and laser diodes.

2.4.1 Polar GaN

In the polar orientation of Gallium Nitride (GaN) crystals, growth typically occurs along the c-axis, which is the most thermodynamically stable direction. This orientation corresponds to the [0001] direction, with the Ga-face (Ga-polar) on one end and the N-face (N-polar) on the opposite end. GaN's wurtzite structure lacks inversion symmetry

along this axis, meaning the crystal has distinct chemical and physical properties depending on which face is exposed.

The Ga-polar face (with gallium atoms terminating the surface) and the N-polar face (terminated by nitrogen atoms) behave differently during crystal growth and subsequent processing. For example, the Ga-polar face tends to be more chemically stable and incorporates p-type dopants (like magnesium) more efficiently, whereas the N-polar face is more reactive and tends to favor the incorporation of n-type dopants.

From a bonding perspective, each atom in the wurtzite structure is tetrahedrally coordinated, forming strong covalent bonds with atoms of the opposite type. However, due to the significant electronegativity difference between gallium (Ga) and nitrogen (N), these bonds also exhibit partial ionic character. Nitrogen, being more electronegative, behaves as an anion, while gallium acts as a cation. This asymmetry in charge distribution leads to a phenomenon known as spontaneous polarization (Psp) along the c-axis. This intrinsic polarization plays a vital part in the optical and electrical behavior of GaN-based devices, especially in heterostructures like quantum wells used in LEDs and high-electron-mobility transistors (HEMTs).

Table 2.1 Lattice Parameters of GaN

Parameters	**GaN**
a_0 (A^0)	3.189
c_0 (A^0)	5.185

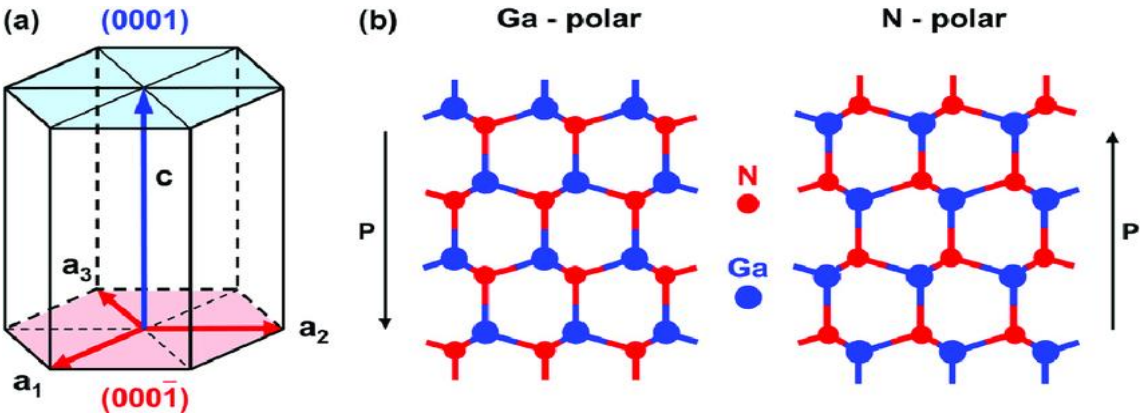

Fig 2.5 (a) Hexagonal Unit Cell (b) Atomic structure of Ga- and N-polar GaN [11]

2.4.2 Non-Polar GaN

The crystallographic orientation and surface polarity of Gallium Nitride (GaN) have a significant impact on the performance of optoelectronic devices, particularly photodetectors. In the non-polar orientation, the crystal plane is oriented at a 90° angle relative to the polar c-plane. While C-plane GaN (polar) is widely used in current GaN-based optoelectronics, it inherently exhibits spontaneous and piezoelectric polarization, which contributes to performance limitations such as lower responsivity and slower response times in devices like photodetectors.

In contrast, non-polar GaN eliminates or significantly reduces these polarization effects. This absence of built-in electric fields enables improved quantum efficiency and faster carrier dynamics, making non-polar GaN a promising candidate for high-performance ultraviolet photodetectors (UV PDs). Furthermore, because non-polar GaN is not subject to the quantum-confined Stark effect (QCSE), which is driven by polarization fields in polar orientations, devices fabricated on non-polar substrates tend to exhibit superior optical and electronic behavior.

In recent years, non-polar GaN has attracted increasing attention for its potential to enhance the efficiency, speed, and stability of various GaN-based optoelectronic applications, making it a strong alternative to traditional polar GaN substrates.

2.4.3 Semi-Polar GaN

Semi-polar GaN represents an intermediate crystal orientation between the polar and non-polar planes. Producing semi-polar GaN substrates is more challenging, as it requires slicing standard polar GaN wafers at specific angles. Several semi-polar planes have been identified, including:

- $(11\bar{2}2)$ inclined at 58° to the c-plane,
- $(10\bar{1}1)$ inclined at 118°,
- $(20\bar{2}1)$ inclined at 75°, and
- another $(20\bar{2}1)$ orientation inclined at 105°.

Although the polarization fields in semi-polar GaN are not completely eliminated, they are significantly reduced compared to polar orientations. This reduced polarization improves carrier recombination rates and supports better charge transport, which is particularly beneficial in light-emitting devices and detectors. As a result, semi-polar GaN has emerged as a promising compromise—offering some of the polarization suppression benefits of non-polar GaN while retaining the higher crystalline quality often associated with polar orientations.

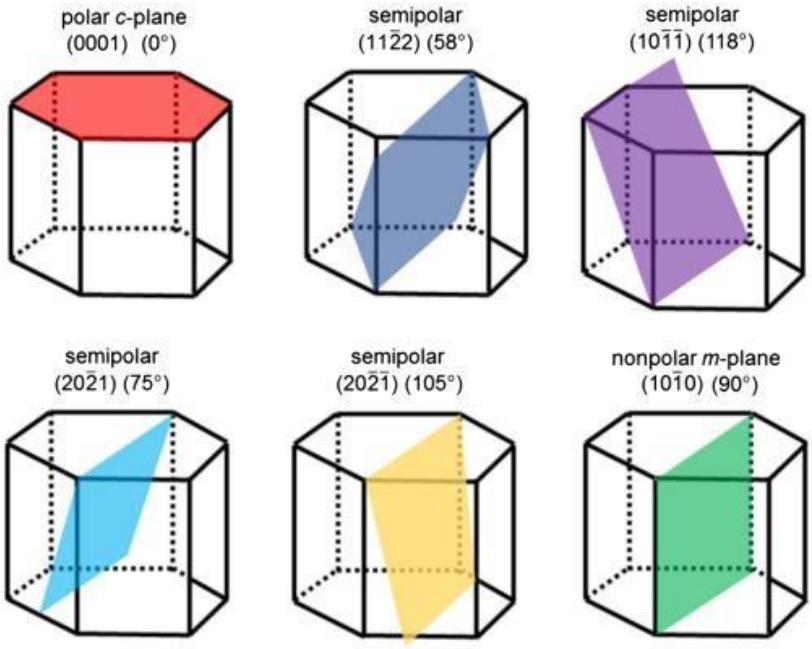

Fig 2.6 Representation of polar, Non-polar, and Semi-polar GaN substrates. [12]

The figure above illustrates the various crystal orientations of GaN, highlighting how the growth direction significantly influences the material's physical and electronic properties. These orientations include polar, semi-polar, and non-polar planes:

- Polar GaN (typically along the c-axis or [0001] direction) exhibits strong spontaneous and piezoelectric polarization effects, which can influence carrier dynamics and optical transitions in devices.
- Semi-polar GaN, grown at specific inclinations to the c-plane, shows reduced but non-negligible polarization fields, making it advantageous for applications requiring improved carrier recombination without fully sacrificing crystal quality.

- Non-polar GaN, oriented perpendicular to the c-axis, effectively eliminates polarization effects, leading to enhanced optical efficiency and faster response in devices by avoiding the quantum-confined Stark effect.

These variations in polarization significantly impact the design and performance of GaN-based optoelectronic devices.

2.5 Indium Nitride (InN)

Indium Nitride (InN) has garnered significant research interest in recent years due to its advantageous optoelectronic properties. Initially believed to have a bandgap of approximately 2.0 eV, more recent studies have revealed that InN possesses a narrower direct bandgap of about 0.7 eV, which significantly broadens its potential for device applications.

The ternary alloy $In_xGa_{1-x}N$, formed by alloying InN with GaN, exhibits a tunable direct bandgap that spans from ultraviolet (3.4 eV for GaN) to infrared (0.7 eV for InN). This wide spectral tunability makes indium-containing III-nitride alloys highly versatile for a broad range of optoelectronic devices.

In particular, InN and its related ternary compounds play a crucial role in the development of high-performance light-emitting diodes (LEDs), photodetectors (PDs), and laser diodes, especially for applications requiring emission or detection across the visible to infrared spectrum.

Moreover, when combined with other III-V binary nitrides such as Aluminum Nitride (AlN) and Gallium Nitride (GaN), InN contributes to the formation of important ternary systems like InGaN and InAlN, further expanding the flexibility and functionality of nitride-based semiconductor technologies.

Table 2.2 Basic properties of III-Nitride Wurtzite structure

Property	**GaN**	**InN**
Lattice Constant, a[A]	3.189	3.533
Lattice Constant, c[A]	5.186	5.693

Band Gap [eV]	3.41	0.7
Electron Affinity [eV]	4.092	5.152
Dielectric Constant	8.9	15.3

2.5.1 Indium Gallium Nitride (InGaN)

Indium Gallium Nitride (InGaN) is a ternary alloy formed by combining Indium Nitride (InN) and Gallium Nitride (GaN)**,** expressed as $In_xGa_{1-x}N$, where *x* represents the mole fraction of indium. It is a direct bandgap III-V semiconductor with a tunable bandgap, making it highly suitable for optoelectronic devices that operate across a wide spectral range—from the infrared (IR) to the ultraviolet (UV). The direct bandgap nature of InGaN allows inter-band transitions to occur without the assistance of phonons, which is critical for efficient light emission.

Vegard's Law and Lattice Constant Estimation

The relationship between the physical properties of InGaN and the indium content *x* can be estimated using Vegard's Law**,** which states that the lattice constant of a binary alloy is a weighted average of its constituents:

$$K_{AxB1-xN} = x*(K_{AN}) + (1-x)*(K_{BN}) \quad (2.1)$$

x is the mole fraction of A, $K_{AN,}$ K_{BN} represents the properties of the materials InN and GaN.

Although Vegard's law provides a linear approximation, real materials often exhibit nonlinear deviations**,** especially in the case of optical properties like bandgap energy. These deviations are corrected using a bowing parameter**.**

2.6 Bandgap Energy of InGaN

The bandgap energy EgE_g of InGaN is composition-dependent and can be estimated using the empirical formula:

$$Eg_{(InxGa1-xN)} = x*Eg_{(InN)} + (1-x)*Eg_{(GaN)} - b*x*(1-x) \quad (2.2)$$

Where $Eg_{(GaN)}$ = 3.41eV, $Eg_{(InN)}$ = 0.7eV, x is the mole fraction of In and b is the bowing parameter (constant).

$$Eg_{(In(x)Ga(1-x)N)} = x*Eg_{(InN)} + (1-x)*Eg_{(GaN)} – b*x*(1-x)$$

$$Eg_{(Inx()Ga(1-x)N)} = x*0.7 + (1-x)*3.41 – 1.43*x8(1-x)$$

This tunability of the bandgap enables InGaN to serve as the core active material in LEDs, laser diodes, and photodetectors**,** particularly in multi-quantum well (MQW) structures for blue, green, and near-UV light emission.

The bandgap of the $In_xGa_{1-x}N$ alloy spans from 0.7 eV to 3.4 eV, effectively covering approximately 90% of the visible spectrum's photon energy range. Due to this wide bandgap tunability, $In_xGa_{1-x}N$ alloy films are capable of absorbing up to 90% of photons with energies above the material’s bandgap within just the first 500 nm of film thickness. This makes them highly efficient absorbers for applications in optoelectronics and photovoltaics.

The growth of InGaN materials is commonly performed using Molecular Beam Epitaxy (MBE). As the indium content increases, so does the strain within the crystal due to the lattice mismatch between InGaN and GaN. This strain becomes more significant at higher indium concentrations, affecting the crystal quality and limiting the achievable layer thickness.

For low indium content, both MBE and Metal-Organic Chemical Vapor Deposition (MOCVD) are effective growth techniques. However, for high indium incorporation, MOCVD becomes less reliable due to issues such as indium segregation and thermal decomposition. In such cases, MBE is preferred because it allows for precise control over growth parameters at relatively lower temperatures, enabling the successful deposition of high-indium-content InGaN layers.

Mole Fraction (x)	Material ($In_xGa_{1-x}N$)	Energy Bandgap (eV)
0	GaN	3.42
0.05	$In_{0.05}Ga_{0.95}N$	3.21607
0.1	$In_{0.1}Ga_{0.9}N$	3.0193
0.2	$In_{0.2}Ga_{0.8}N$	2.6472
0.4	$In_{0.4}Ga_{0.6}N$	1.9888
0.6	$In_{0.6}Ga_{0.4}N$	1.4448
0.8	$In_{0.8}Ga_{0.2}N$	1.1052
1	InN	0.7

Table 2.3 Energy Bandgap (eV) of $In_xGa_{1-x}N$ at mole fraction x

2.7 Synopsys Sentaurus TCAD

Synopsys created the full suite of technology computer-aided design (TCAD) tools known as Synopsys Sentaurus TCAD. These tools are specifically designed to facilitate the modeling, simulation, and optimization of semiconductor fabrication processes and device performance. Sentaurus TCAD enables researchers and engineers to investigate both the structural and electrical characteristics of a wide range of semiconductor devices by numerically solving fundamental physical models.

The Sentaurus environment supports a variety of semiconductor technologies, including silicon-based and compound semiconductor devices (such as GaN, InGaN, AlGaN, etc.). Among the core components of the tool suite are:

1. Sentaurus Workbench (SWB)
2. Sentaurus Device

2.7.1 Sentaurus Tool Flow

The general simulation flow in Sentaurus TCAD involves the following steps:

Sentaurus Structure Editor (SDE):
This module is used to construct the geometric structure of the semiconductor device. It allows the definition of layers, doping profiles, contacts, and mesh generation. The editor outputs a mixed-element grid suitable for electrical and optical simulations.

Sentaurus Device (SDevice):
This tool is responsible for the physical simulation of the device behavior, solving coupled differential equations (Poisson, continuity, heat, etc.) to model electrical and optical characteristics under various operating conditions.

Sentaurus Visual (SVisual):
SVisual is used to post-process simulation data stored in .tdr files. It allows users to extract and visualize electrical, optical, and thermal properties such as current density, carrier distribution, recombination rates, and more.

Sentaurus Workbench (SWB)

Sentaurus Workbench (SWB) provides an integrated graphical user interface (GUI) that consolidates all simulation tools into a single environment. It supports the creation, parameterization, execution, and evaluation of complex simulation workflows. SWB simplifies the overall simulation process by allowing users to:

- Manage multiple simulations on the same or different device structures.
- Define and adjust input parameters for physical models and geometries.
- Automate the execution of simulation steps by sequentially linking tools (e.g., structure → device → visualization).
- Review and analyze simulation results without manual intervention.

This integrated workflow significantly enhances simulation efficiency and reproducibility by automatically generating and transferring required input/output files between tools.

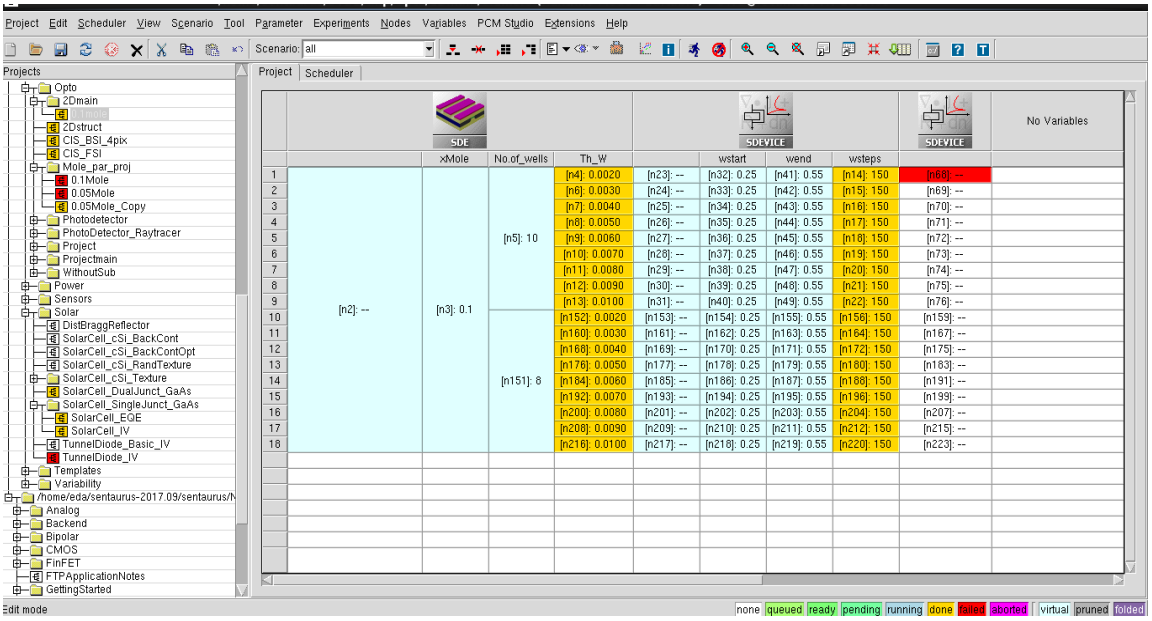

Fig 2.7 Sentaurus Workbench Tool

2.7.2 Sentaurus Structure Editor (SDE)

The Sentaurus Structure Editor (SDE) is a powerful device design tool that allows users to construct both 2D and 3D device structures for use in simulations. Structures can be created using Sentaurus' native format or through user-defined formats, offering flexibility in design. Simulations can be initiated via a graphical user interface (GUI) or through a script-based input written in the Scheme programming language**.**

One of the key features of SDE is its parametric flexibility—users can define physical characteristics or dimensions as variables, enabling parametric sweeps and design optimization. This capability supports the testing of a wide range of device configurations under different conditions.

The structure is discretized using a mesh, which is essential for solving physical equations accurately. This mesh divides the device into smaller elements, allowing detailed modeling of doping profiles, material interfaces, and other physical characteristics. The output from SDE includes detailed information on geometry, materials, doping profiles, contacts, and physical parameters**,** and is passed on to Sentaurus Device (SD) for simulation

2.7.3 Sentaurus Device (SD)

A multidimensional semiconductor device simulator is called Sentaurus Device (SD) that numerically solves a set of coupled partial differential equations, such as Poisson's equation, carrier continuity equations, and transport modelsIt is employed to examine the optical, thermal, and electrical characteristics of semiconductor devices. across a range of materials, including compound semiconductors like GaN and InGaN.

This tool supports a wide variety of physical models, material parameters, and boundary conditions, and employs robust numerical techniques and solvers. The output includes spatial and temporal distributions of key parameters such as:

- Carrier concentrations
- Electric fields and potentials
- Quasi-Fermi levels
- Recombination rates
- Temperature profiles

Sentaurus Device also supports advanced modeling of modern logic and memory technologies, making it suitable for both research and industrial applications.

2.7.4 Sentaurus Visual (SVisual)

Sentaurus Visual (SVisual) is the visualization tool used to interpret and analyze the results of TCAD simulations. It enables detailed inspection of 1D, 2D, and 3D simulation data obtained from Sentaurus Device. Users can interact with the data through both a GUI and scripting environment.

Key features of SVisual include:

- Rendering of device structures and simulation results
- Plotting of physical quantities such as electric fields, carrier densities, and energy bands
- Data extraction and analysis tools, including cross-section views and overlays
- Curve inspection using Inspect, a tool within SVisual that allows plotting and comparison of datasets using coordinate mappings

SVisual facilitates intuitive understanding of complex device behavior and supports data export**,** image generation**,** and report creation for publication or documentation.

2.8 Quantum Well

A quantum well is a type of semiconductor heterostructure formed by sandwiching a thin layer of a narrower bandgap semiconductor (the "well") between two layers of wider bandgap semiconductors (the "barriers"). This layered structure enables quantum mechanical confinement of charge carriers—electrons and holes—within the well region.

In the context of light-emitting diodes (LEDs**)**, quantum wells play a critical role in carrier confinement. The barriers on either side of the well inhibit carrier escape, causing electrons and holes to recombine within the well**.** Unlike traditional p–n junction diodes**,** where the recombination is governed by the diffusion length (typically 1–20 μm), quantum wells restrict recombination to the well thickness**,** which usually ranges from 0.1 to 1 μm. This confinement leads to a higher carrier concentration in the active region and significantly enhances the radiative recombination rate, resulting in more efficient light emission [9].

In bulk semiconductors, energy states in the conduction and valence bands are considered to form a continuous spectrum. However, when the layer thickness is reduced to the nanoscale (as in quantum wells), quantization of energy levels occurs due to quantum confinement. The energy bands are replaced by discrete sub-bands, and the electronic properties must be described using quantum mechanics**.**

The discrete energy levels in a quantum well are derived from the time-independent Schrödinger equation**:**

$$-\frac{(h^2)\cdot d^2\phi\cdot n}{2\cdot m\cdot dz^2} + V(z)\cdot \phi_n = \mathrm{E_n}\phi_n \qquad (2.3)$$

Where:

- h is Planck’s constant,
- m is the effective mass of the carrier (electron or hole),
- V(z) is the potential energy function across the heterostructure,
- Φn is the wave function of the nth energy state,

- En is the energy of the nth level.

Two common methods are used to solve this equation:

- Infinite potential well: Assumes that the barriers are infinitely high, resulting in quadratically spaced energy levels and sine wave solutions inside the well.
- Finite potential well**:** More realistic, with finite barrier heights**.** In this case, Within the well, the wave functions are sine waves, but when they approach the barriers, they show exponential decay.

A structure comprising multiple quantum wells is termed **a** multi-quantum well (MQW)**.** When the wave functions of adjacent wells overlap**,** a superlattice is formed. This overlap leads to the formation of mini bands, allowing carrier transport through quantum tunneling**.**

It is also important to note that optical transitions in quantum wells are governed by selection rules: transitions occur only between energy states with the same quantum number**,** preserving the symmetry of the wavefunction.

2.9 Light Emitting Diode

When an electric current is supplied, a Light Emitting Diode (LED), an optoelectronic semiconductor device based on a p–n junction, emits light. It uses a two-stage technique to transform electrical energy into optical energy. that leverages the principles of carrier injection and radiative recombination.

An LED structure typically consists of a p-type and n-type semiconductor material placed in close contact to form a p–n junction**,** the fundamental region responsible for light emission. The wavelength (and thus the color) of the emitted light is primarily determined by the bandgap energy of the semiconductor material used.

Operating Principle:

1. **Carrier Injection**: Electrons from the n-side and holes from the p-side are introduced into the junction region when a forward bias is applied across the p–n junction. These carriers are raised above their thermal equilibrium state using the supplied electrical energy.

2. **Radiative Recombination**: After a short time (mean lifetime), the electrons in the conduction band recombine with holes in the valence band, releasing energy in the form of spontaneous photon emission**.** The energy of the emitted photon corresponds approximately to th**e** bandgap energy **(**Eg**)** of the material.

In addition to photon emission, a tiny percentage of carriers who are minority may recombine non-radiatively**,** releasing energy in the form of phonons (heat), which contributes to the thermal losses in the device.

Photon Energy and Wavelength:

The energy of the emitted photon is governed by **Planck's relation**:

$$\Delta E = h \cdot v = \frac{hc}{\lambda} \tag{2.4}$$

Thus, the wavelength of the emitted light can be directly related to the bandgap energy of the semiconductor material. For instance, a semiconductor with a bandgap of 2 eV will emit light at approximately 620 nm, which lies in the red region of the visible spectrum.

2.9.1 Carrier Generation in LEDs

In LEDs, carrier generation primarily occurs via electrical injection. When a forward bias is applied across the p-n junction, electrons from the n-type region and holes from the p-type region are injected into the active region, typically a quantum well or multi-quantum well (MQW) layer. This injection process creates a non-equilibrium carrier population, raising electrons to the conduction band and creating corresponding holes in the valence band.

Unlike photovoltaic devices, generation in LEDs is not driven by light absorption, but by carrier injection through an external power supply. The efficiency of carrier injection is influenced by the band alignment, doping concentrations, and contact resistance at the p- and n-interfaces.

2.9.2 Recombination Mechanisms

Once carriers are generated and confined in the active region, recombination occurs through several competing processes:

2.9.2.1 Radiative Recombination

This is the desirable recombination mechanism in LEDs, where an electron from the conduction band recombines with a hole in the valence band, emitting a photon with energy approximately equal to the bandgap of the semiconductor. Radiative recombination is most efficient when:

- Carrier confinement is high (e.g., in quantum wells)
- The material has a direct bandgap (like GaN or InGaN)
- Defect levels are minimal

Radiative recombination rate is given by:

$$R_{spon} = B(n \cdot p - n_o \cdot p_o) \tag{2.5}$$

2.9.2.2 Shockley–Read–Hall (SRH) Recombination

This is a non-radiative recombination mechanism involving defect or trap states within the bandgap, usually introduced during material growth or due to dislocations. Electrons and holes recombine via these mid-gap states, releasing energy as heat rather than light. SRH recombination is more prominent in materials with high defect densities or poor crystal quality.

The SRH recombination rate is given by:

$$R_{net}^{SRH} = \frac{np - n_{i,pxf}^2}{\tau_p(n+n_1) + \tau_p(p+p_1)} \tag{2.6}$$

2.9.2.3 Auger Recombination

This is a higher- a non-radiative process that transfers an electron-hole pair's recombination energy to a third carrier (electron or hole), which is then excited to a higher energy state and eventually thermalizes. Auger recombination is significant at high carrier densities and contributes to efficiency droop in high-power LEDs.

Auger recombination rate:

$$R_{net}^{A} = (C_n \cdot n + C_p \cdot p)(np - n^2 \text{ i,eff}) \qquad (2.7)$$

2.10 Ray Tracing

In LED devices, when photons are generated through electron-hole recombination in the active region, not all of them contribute to the external optical output. This is due to the inherent optical properties of the device, such as reflection, transmission, and absorption at material interfaces. When a light ray encounters a boundary between materials with different refractive indices, portions of it may be reflected back, transmitted through, or absorbed depending on the optical characteristics of the interface.To accurately model this behavior, Sentaurus Device uses a ray tracing algorithm that tracks the paths of photons generated inside the device. This method employs a recursive approach, starting with an initial light ray and building a binary tree based on whether the ray is reflected or transmitted at each interface. The key factor determining these interactions is the refractive index mismatch at material boundaries.

The optical output power is calculated by summing the powers of all the rays that exit the device through a defined extraction window. This allows for precise estimation of how much internally generated light is actually emitted from the device.LED simulations require both electrical and optical modeling. The electrical part involves solving the Poisson and carrier continuity equations, which provide the carrier densities in the active region. These carrier densities are used in recombination models to determine the spontaneous emission rate, which in turn feeds into the ray tracing model.

Next, this power of spontaneous emission is utilized as the source for ray tracing, enabling the computation of optical intensity and the analysis of light extraction efficiency. By combining electrical and optical models, Sentaurus Device provides a comprehensive simulation of LED performance, covering carrier transport, photon generation, and light output behavior.

3

CALCULATION OF OPTICAL PROPERTIES OF III-V NITRIDES

Chapter 3

3.1 Introduction

The main topic of this chapter is analyzing the optical properties of the ternary alloy $In_xGa_{1-x}N$, particularly the complex refractive index as a function of the indium mole fraction (x) across various wavelengths. The study emphasizes how the cut-off wavelength and the extinction coefficient evolve with changes in the indium composition. These variations are essential to understand for accurately designing and modeling optoelectronic devices such as LEDs and photodetectors that are based on InGaN/GaN heterostructures.

3.2 Complex Refractive Index of $In_xGa_{1-x}N$

III-V nitride semiconductors, including GaN and its ternary alloy InGaN, are widely used in optoelectronics due to their ability to cover a broad spectral range—from ultraviolet (~0.2 μm) to near-infrared (~1.1 μm). Gallium Nitride (GaN) features a direct bandgap of approximately 3.42 eV, while the bandgap of the $In_xGa_{1-x}N$ alloy can be tuned from 3.4 eV (x = 0) down to around 0.7 eV (x = 1), depending on the indium content.Although InGaN/GaN quantum well structures are central to modern light-emitting and detection technologies, their optical behavior is still not fully characterized, particularly in terms of the complex refractive index. Accurate modeling of these properties is crucial for simulating light-matter interaction and optimizing device performance.

To address this, Sentaurus Device provides a sophisticated model that calculates the complex refractive index of materials. This model takes into account multiple physical parameters such as indium mole fraction (x), local optical gain, wavelength, carrier concentration, and temperature. From this, it computes both both the imaginary and real components of the refractive index (n), known as the extinction coefficient (k), which relates to absorption losses within the material.

This theoretical framework enables engineers and researchers to precisely evaluate how variations in alloy composition and device operating conditions affect light propagation and absorption in InGaN-based devices.

The complex refractive index of the material can be written as :

$$\tilde{n} = n + i.\mathrm{k} \tag{3.1}$$

The refractive index of InxGa1xN as a function of the refractive index of GaN and InN follows the same Vegard's law as the bandgap.

$$H_{InxGa1-xN} = \eta_{InNx} + (1 - x)*\eta_{GaN} - b*x*(1 - x) \tag{3.2}$$

Where η is the refractive index, x is the mole fraction ,

b is the bowing parameter having value is 1.43.

The dispersion behavior of refractive indices in III-nitride binary and ternary alloys is of considerable significance, complementing the understanding of their band structure properties. Several approaches have been introduced in the literature to model the refractive index in such alloy semiconductors. Among them, empirical oscillator-based models are frequently employed to estimate the refractive index variation at photon energies below the material's bandgap.

A more physically grounded approach was proposed by Adachi in 1982, wherein a model was developed to describe the dielectric function of dielectric and semiconductor materials. This model is particularly applicable within the transparency spectral region that is, the range where photon energies are less than the semiconductor bandgap (E < Eg). It offers a more accurate theoretical basis for analyzing how the refractive index behaves in non-absorptive spectral regions, especially for materials like InGaN used in optoelectronic devices.

$$\text{NWHICH} = \sqrt{A\left[\frac{E_{ph}}{E_g}\right]^{-2}\left[2 - \sqrt{1 + \left[\frac{E_{ph}}{E_g}\right]} - \sqrt{1 + \left[\frac{E_{ph}}{E_g}\right]}\right] + B} \tag{3.3}$$

$$A(In_xGa_{(1-x)}N) = 13.55*x + 9.31*(1-x)$$

$$B(In_xGa_{(1-x)}N) = 2.05*x + 3.03*(1-x)$$

The refractive index of a material typically varies with photon energy, and this relationship is often modeled using fitting parameters, commonly denoted as *A* and *B*. These parameters are not fixed but instead depend on the composition of the alloy, which directly influences the material's bandgap. This method has been widely adopted in modeling optical properties of III-nitride binary compounds such as AlN, GaN, and InN, and has proven effective in aligning with experimental observations.For ternary alloys, the refractive

index can be estimated through a linear interpolation of the *A* and *B* values corresponding to the constituent binary materials. This approach simplifies the calculation while maintaining reasonable accuracy.

Additionally, the imaginary part of the complex refractive index, often referred to as the extinction coefficient, plays a key role in determining the material's absorption behavior. Specifically, it is directly linked to the absorption coefficient, which quantifies how much light is absorbed as it propagates through the medium.

$$A = 4*\pi*k/\lambda \tag{3.4}$$

In this context, the absorption coefficient (denoted as α) describes how strongly a material absorbs light at a given wavelength. It is related to the extinction coefficient (*k*), which is the imaginary part of the complex refractive index, and the wavelength of the incident light (*λ*). The relationship between these parameters is essential for analyzing the optical behavior of semiconductors.

To determine the absorption characteristics of $In_xGa_{1-x}N$ alloys, wavelength-dependent absorption coefficients were calculated for various indium compositions. Specifically, compositions of *x* = 1, 0.83, 0.69, 0.57, 0.5, and 0 were considered, covering a range from pure InN to pure GaN. This allows for a comprehensive understanding of how varying indium content influences light absorption in these ternary alloys.

$$A(In_xGa_{1-x}N) = 10^5\sqrt{C\left[E_{ph} - E_g\right] + D\left[E_{ph} - E_g\right]^2} \tag{3.5}$$

E_{ph} is the Energy of incident photon and E_g is bandgap of $In_xGa_{(1-x)}N$ Where C and D are fitting parameters, that is given by:

$$C(In_xGa_{(1-x)}N) = 3.525 - 18.29*x + 40.22*x^2 - 37.52*x^3 + 12.77*x^4 \tag{3.6}$$

$$D(In_xGa_{(1-x)}N) = -0.665 + 3.616*x - 2.460*x^2 \tag{3.7}$$

$$k = \lambda\alpha/4\pi$$

Indium composition	C	D
1	0.69642	0.46055
0.83	0.66796	0.68886
0.69	0.58108	0.66902
0.57	0.60946	0.62182
0.5	0.51672	0.46836
0	3.52517	−0.65710

Table 3.1 $In_xGa1-xN$ alloys absorption coefficient computation using fitting parameters

The equation to solve electron effective mass of an electron and hole for the given mole fraction is given by:

$$m_n\,(In_xGa_{(1-x)}N) = 0.12*x + 0.2*(1-x)$$

$m_h\,(In_xGa_{(1-x)}N) = 0.17*x + 1.0*(1-x)$ where m_n and m_h are effective mass of electron and hole respectively.

Mole Fraction (x)	Material ($In_xGa_{1-x}N$)	Effective mass of electron	Effective mass of hole
0	GaN	0.2	1
0.05	$In_{0.05}Ga_{0.95}N$	0.196	0.9585
0.1	$In_{0.1}Ga_{0.9}N$	0.192	0.917
0.2	$In_{0.2}Ga_{0.8}N$	0.184	0.834
0.4	$In_{0.4}Ga_{0.6}N$	0.168	0.668
0.6	$In_{0.6}Ga_{0.4}N$	0.152	0.502
0.8	$In_{0.8}Ga_{0.2}N$	0.136	0.336
1	InN	0.12	0.17

Table 3.2 Effective mass of electron and hole of $In_XGa_{(1-x)}N$ w.r.t change in mole fraction x

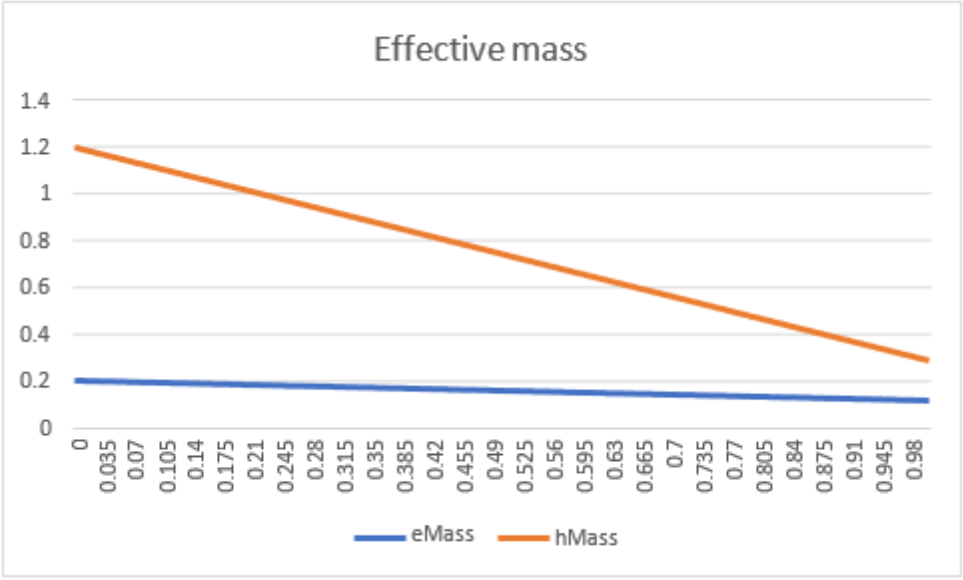

Fig 3.3 Effective mass of electron and hole of $In_xGa_{(1-x)}N$ for mole fraction x

The above fig shows the variations of effective mass of electron and hole with respect to change in mole fraction. As the mole fraction increases the effective mass of electron and hole increases.

Complex Refractive Index values of $In_xGa_{1-x}N$ w.r.to mole fraction:

x = 0.05 i.e, $In_{0.05}Ga_{0.95}N$:

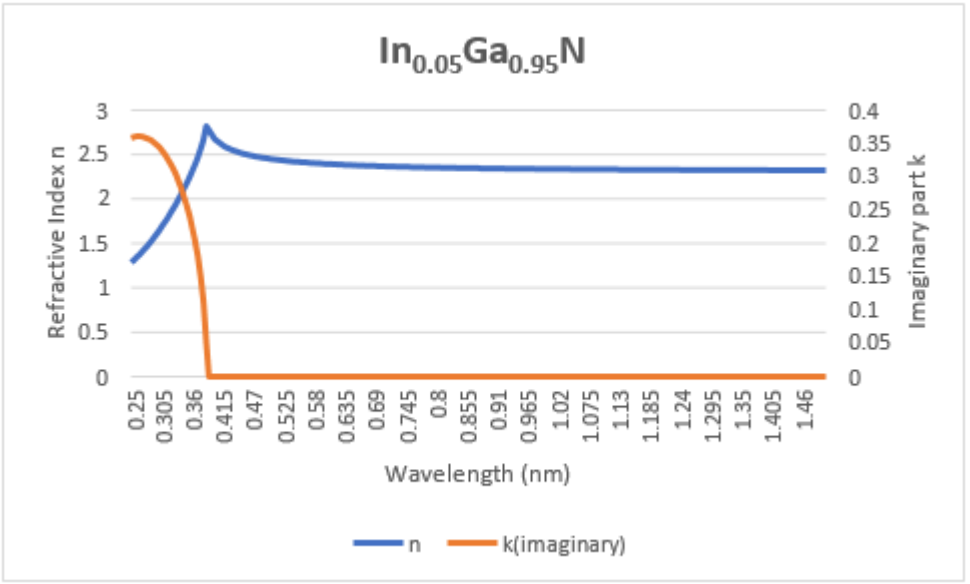

Fig 3.2 Complex Refractive Index of $In_{0.05}Ga_{0.95}N$ vs Wavelength (nm)

In the above fig, For the mole fraction of 5% In i.e, for In0.05Ga0.95N the cut off wavelength for absorption is 385nm.

At x = 0.1 i.e, $In_{0.1}Ga_{0.9}N$:

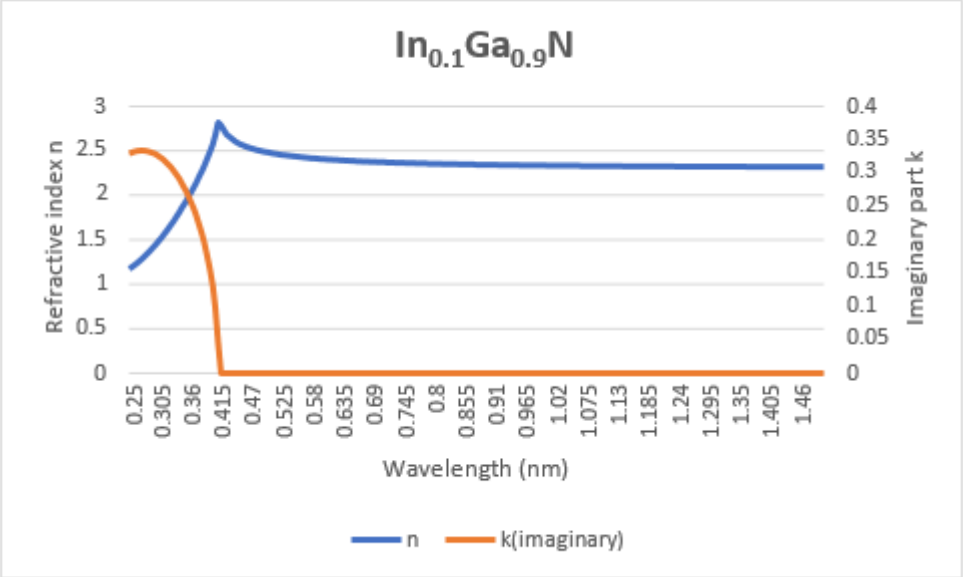

Fig 3.3 Complex Refractive Index of In0.1Ga0.9N vs Wavelength (nm)

In the above fig, For the mole fraction of 5% In i.e, for In0.1Ga0.9N the cut off wavelength for absorption is 410nm.

At x = 0.2 i.e, $In_{0.2}Ga_{0.8}N$:

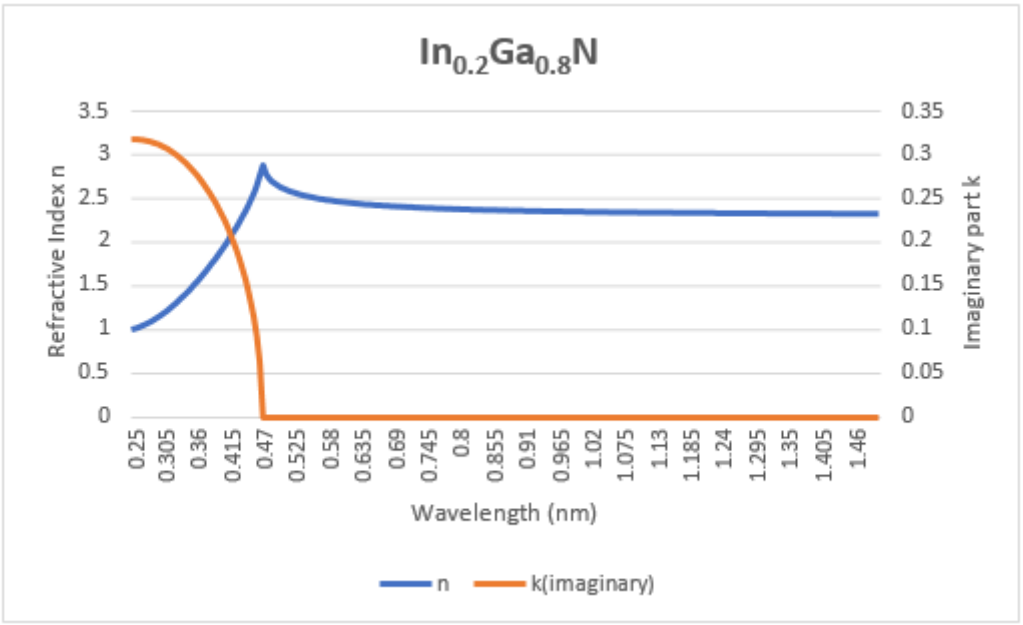

Fig 3.4 Complex Refractive Index of $In_{0.2}Ga_{0.8}N$ vs Wavelength (nm)

3.3 Polarization Effects in Group III-Nitride Heterostructures

Polarization effects are quite important in the behavior and performance of Group III-nitride semiconductors. These materials are typically grown along the *c*-axis of the hexagonal wurtzite crystal structure—a direction known to exhibit strong polarization phenomena. This is largely attributed to the non-centrosymmetric nature of the wurtzite lattice combined with the high ionicity of the metal–nitrogen bond in compounds like GaN and InN. In these materials, two main types of polarization are observed: spontaneous polarization, which occurs naturally due to the crystal structure, and piezoelectric polarization, which arises from strain in the lattice, especially at interfaces in heterostructures. Both types of polarization can significantly influence the optical and electronic characteristics of GaN-based devices. In fact, III-nitrides possess some of the largest polarization coefficients among semiconductor materials, making these effects particularly pronounced.

The high degree of piezoelectric polarization observed in *c*-plane oriented structures is a direct result of the large difference in electronegativity between gallium (Ga) and nitrogen (N). Since nitrogen is more electronegative, it tends to attract more electrons, leading to a net negative charge near the nitrogen atoms and a positive charge near the gallium atoms. This separation of charge gives rise to a built-in electric field along the growth direction.

One of the key consequences of internal polarization fields is the Quantum Confined Stark Effect (QCSE). In quantum wells (QWs), these fields tilt the potential profile, reducing the overlap between electron and hole wave functions. As a result, radiative recombination becomes less efficient, leading to a drop in internal quantum efficiency (IQE).

The presence of QCSE poses significant challenges, especially in optoelectronic devices like light-emitting diodes (LEDs) and photodetectors grown along the *c*-plane. To mitigate these effects, researchers have proposed growing devices along alternative crystallographic orientations that exhibit reduced or negligible polarization fields—such as semi-polar or non-polar planes. By minimizing internal electric fields, these orientations help enhance wavefunction overlap and boost device performance.

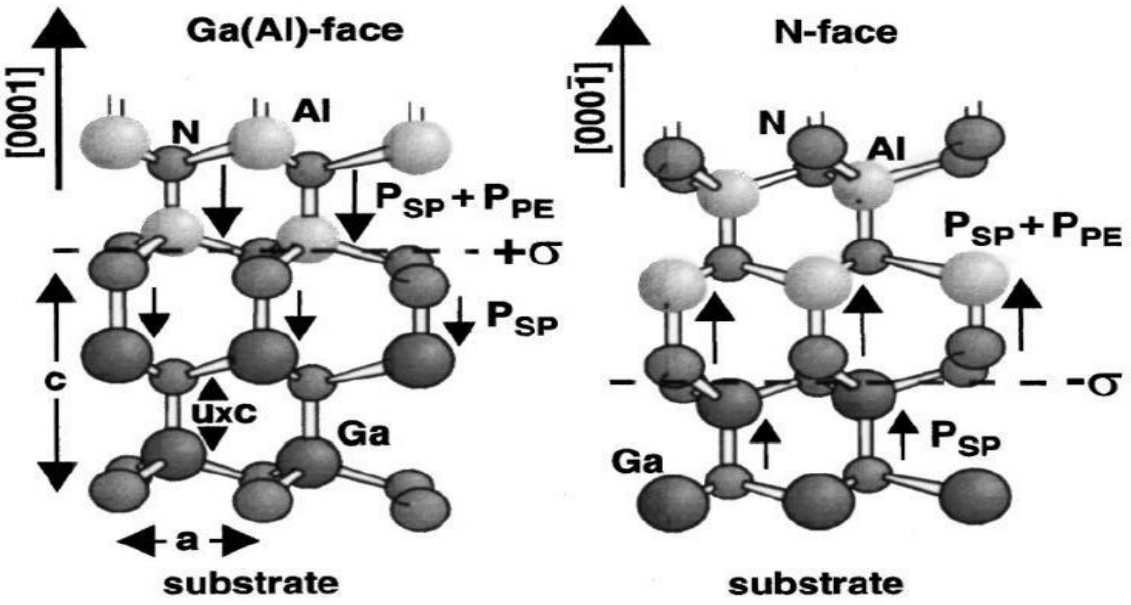

Fig 3.5 Shows the Polarization along the c-axis [18]

The figure above illustrates the polarization effects in GaN material, primarily driven by the significant difference in electronegativity between nitrogen and gallium atoms. This disparity leads to the formation of internal polarization fields within the crystal structure.

Two main components contribute to the overall polarization in GaN: spontaneous polarization (PSP) and piezoelectric polarization (PPE).

- Spontaneous polarization arises intrinsically from the wurtzite crystal structure of GaN, even in the absence of any external mechanical stress or electric field. It is a result of the inherent asymmetry and ionicity of the Ga–N bond.
- Piezoelectric polarization on the other hand, is induced by mechanical strain due to lattice mismatches between different layers—most notably between the quantum wells, barrier layers, and the underlying substrate. When these layers are epitaxially grown, the strain generates additional polarization through the piezoelectric effect.

Together, these polarization fields play a significant role in modifying the internal electric field across heterojunctions, which directly affects the optical and electronic behavior of GaN-based devices.

4

PROPOSED STRUCTURE DESIGN

Chapter 4

4.1 Introduction

The previous chapters highlighted the critical role of polarization effects, material orientation, and indium composition on the performance of Group III-nitride optoelectronic devices. In this chapter, a robust LED structure based on the $In_xGa_{1-x}N$/GaN multiple quantum well (MQW) system is proposed. This design aims to optimize the optical and electrical efficiency by addressing material challenges such as threading dislocations, quantum well confinement, and photon absorption.

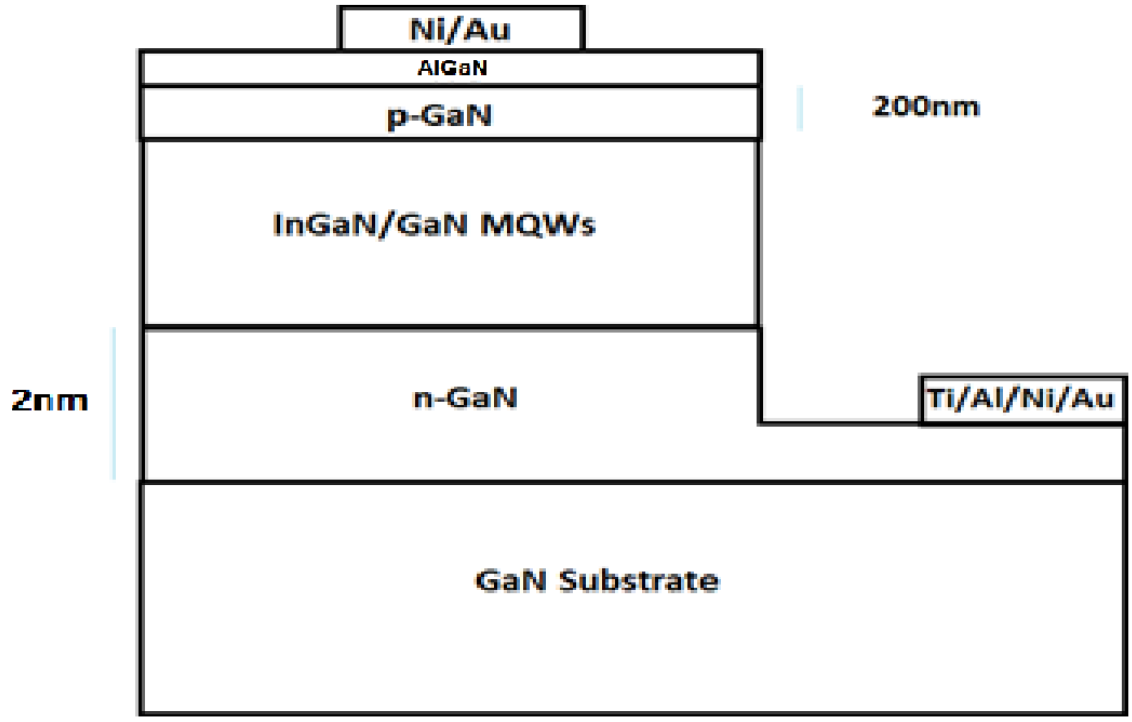

Fig 4.1 LED structure employed for modeling.

4.2 Device Configuration

The proposed LED utilizes a p-i-n heterojunction layout, integrating multiple quantum wells composed of $In_xGa_{1-x}N$ wells and GaN barriers. The choice of materials is based on their high internal quantum efficiency and bandgap tunability. Indium-rich InGaN wells, sandwiched between GaN barriers, serve as active regions for photon generation.

The GaN substrate is selected over sapphire due to its lower threading dislocation density and superior thermal/electrical conductivity, thereby supporting higher quality epitaxial growth and improved carrier mobility. The intrinsic region includes 10 pairs of MQWs, optimized for UV-blue emission around 370–410 nm. The n-type GaN is doped with silicon (~4e+19 cm^{-3}) and p-type GaN is doped with magnesium (~3.8e+17 cm^{-3}). A high-transmission ITO layer is deposited atop the p-GaN to serve as a transparent electrode.

4.3 Structural Design and Fabrication Considerations

The quantum wells are designed to be 4 nm thick, while the barriers are 10 nm. These values ensure sufficient quantum confinement and reduce carrier escape. The active layer configuration is tailored using Vegard's law to adjust indium content, which affects the emission wavelength. For instance, ~10% indium content supports emission near 410 nm. To form ohmic contacts, Al/Ti/Ni/Au (60/20/30/70 nm) metals are used for the n-contact, and Ni/Au (10/30 nm) for the p-contact. These materials are selected for their proven compatibility with GaN and reliable contact resistance.

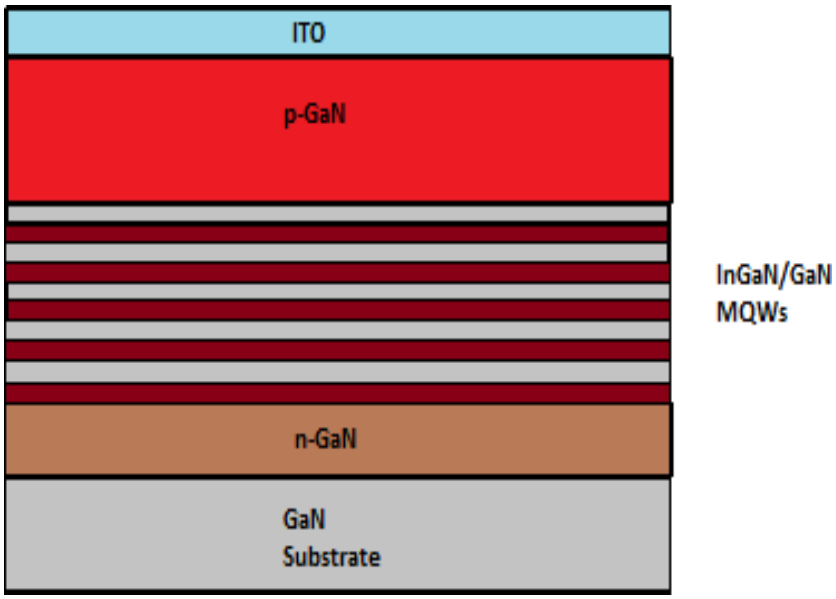

Fig 4.2 Multiple Quantum Well LED

4.4 Final Optimized Parameters

Parameter	Optimized Value
Substrate	GaN (350 µm)
n-GaN Layer Thickness	2 µm
p-GaN Layer Thickness	200 nm
InGaN Well Thickness	4 nm
GaN Barrier Thickness	10 nm
Indium Content in InGaN	8–10% (for 370–410 nm)
Number of MQWs	5
EBL (AlGaN)	10 nm
ITO Layer Thickness	100 nm
Contacts (n-type)	Al/Ti/Ni/Au
Contacts (p-type)	Ni/Au

These parameters ensure a balance between material constraints and desired optical output. The design aims to be fabrication-ready and scalable for high-volume applications.

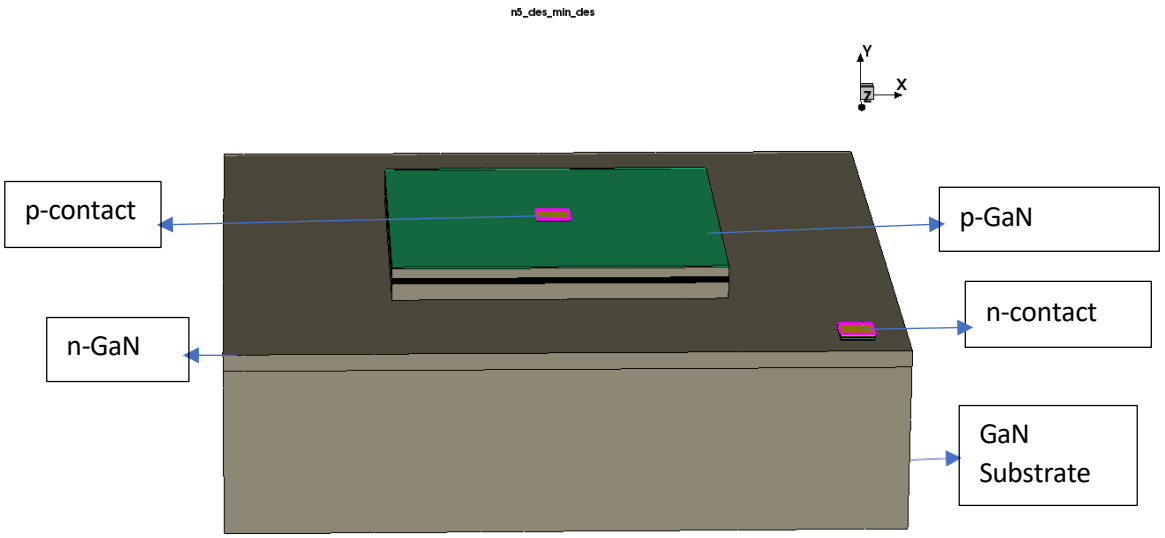

Fig 4.3 Developed 3D Light Emitting Diode

5

RESULTS AND DISCUSSION

Chapter 5

5.1 Band Diagram

The band structure of the Designed LED is simulated, the conduction and valence band levels are shown in Fig 5.1

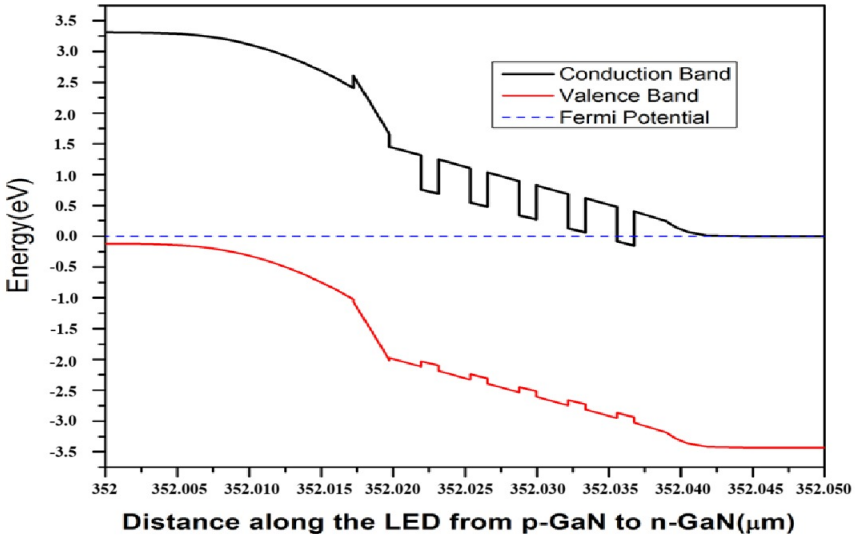

Fig 5.1 Band diagram of the LED device plotted along the lateral direction of LED.

The conduction and valence band profiles shown in Figures 5.1 illustrate the formation of a distinct quantum well structure. This well plays a vital role in confining charge carriers—electrons and holes—within the active region. Such confinement within the InGaN quantum well significantly increases the chances of radiative recombination, which is essential for efficient light emission in LED devices.

5.2 Distribution of electrons and holes from p-GaN to n-GaN along the LED in Presence and Absence of AlGaN EBL.

In Presence of AlGaN EBL

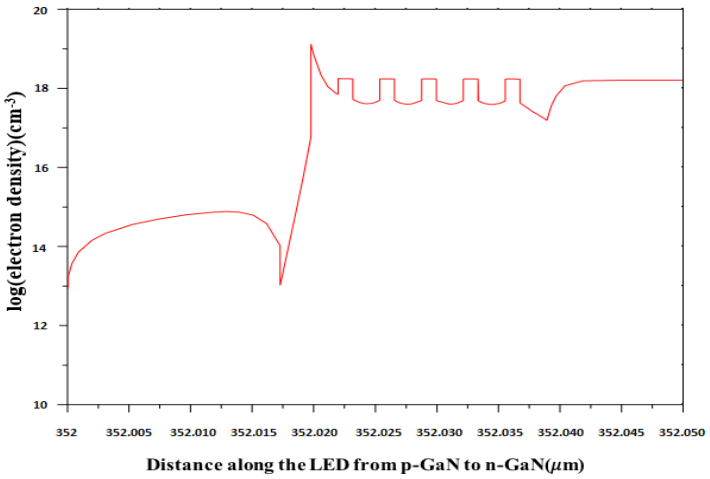

In Absence of AlGaN EBL

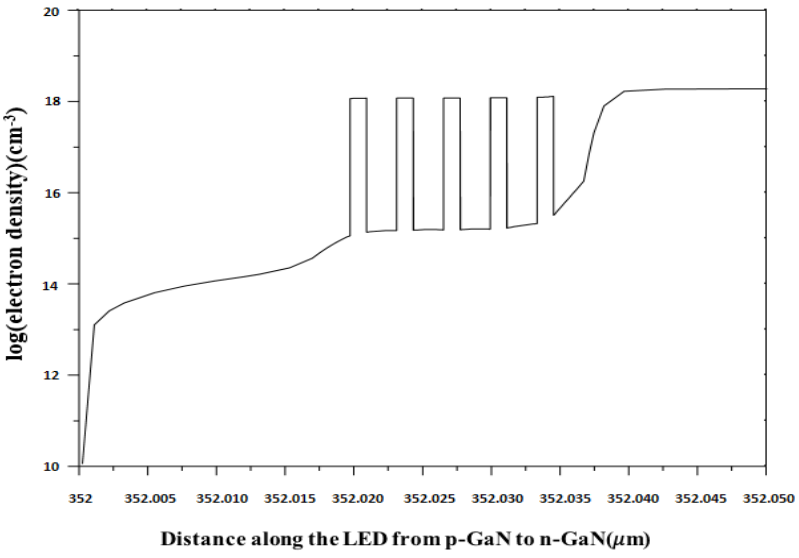

Fig 5.2 Distribution of electrons from p-GaN to n-GaN along the LED.

In presence of AlGaN EBL

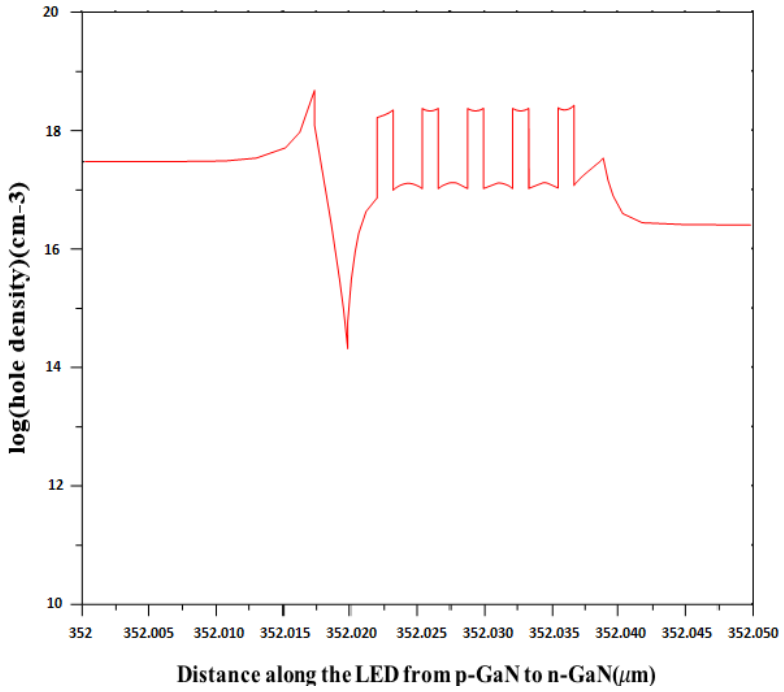

In Absence of AlGaN EBL

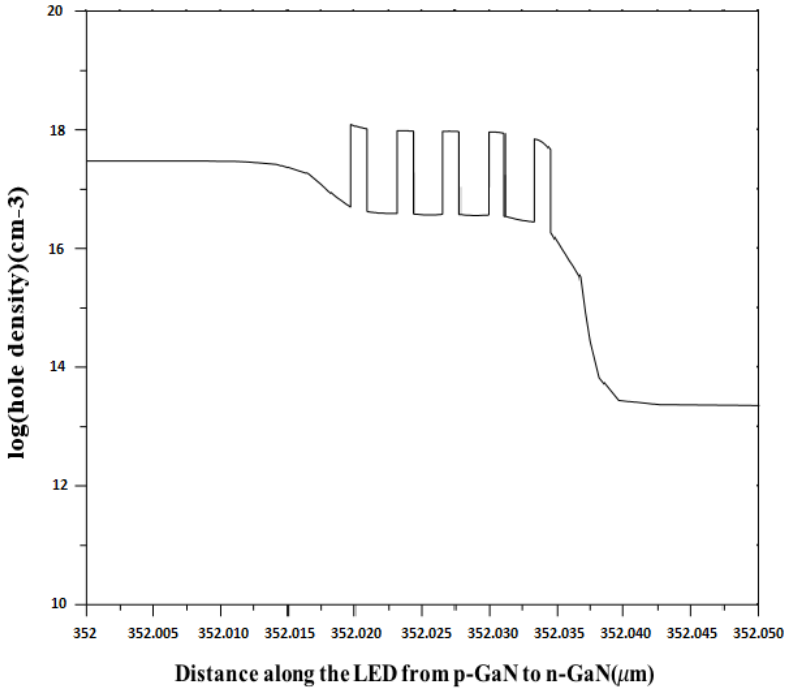

Fig 5.3 Distribution of holes from p-GaN to n-GaN along the LED

5.3 Rates of radiative recombination, hole distribution, and electron distribution in the LED with different Al composition in AlGaN EBL

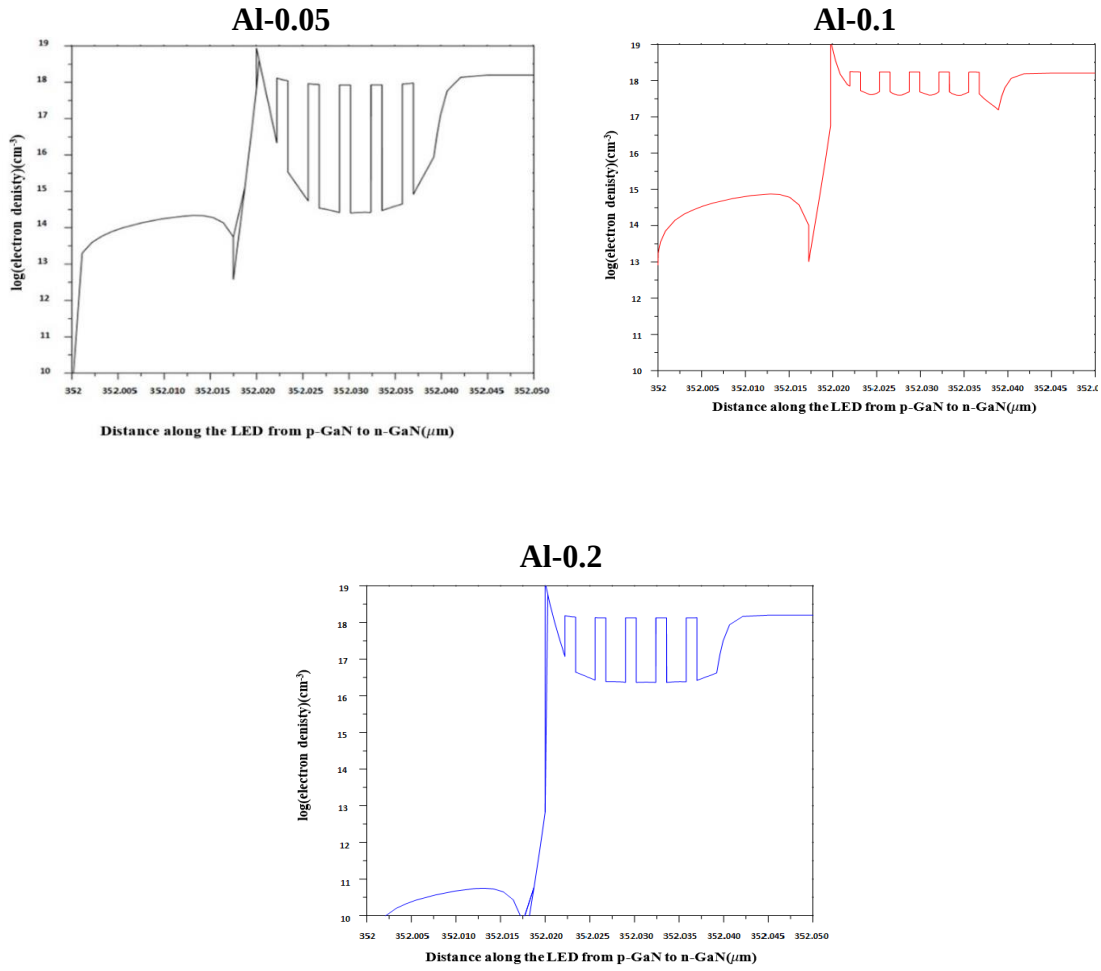

Fig 5.4 Electron distribution rate in the LED with different amounts of Al.

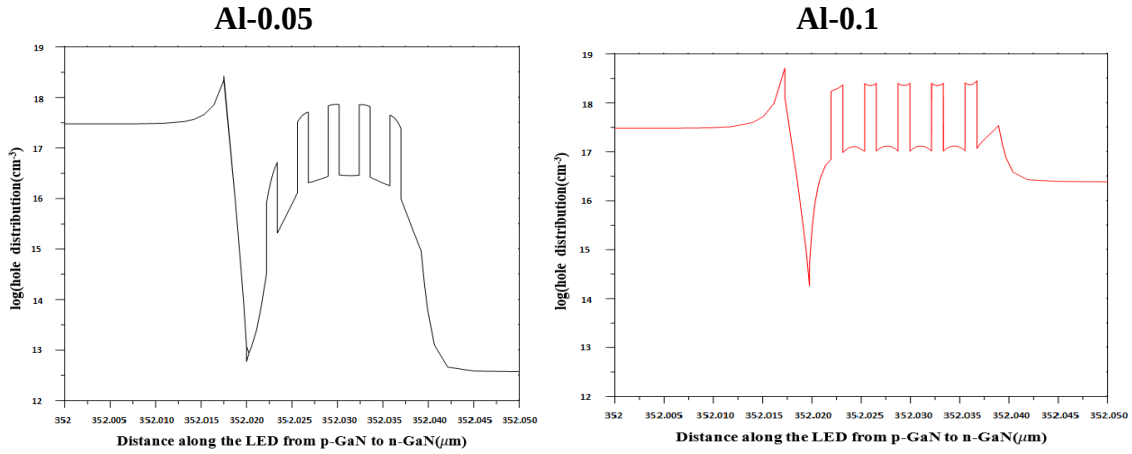

Al-0.2

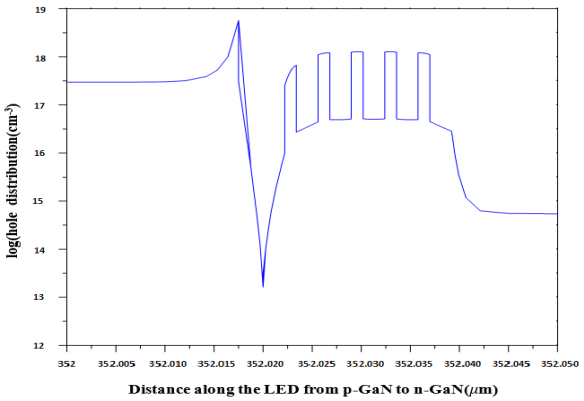

Fig 5.5 Hole distribution rate in the LED with different amounts of Al.

Al-0.05

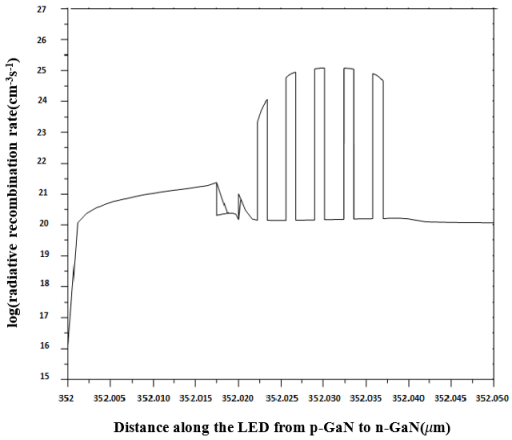

Al-0.1

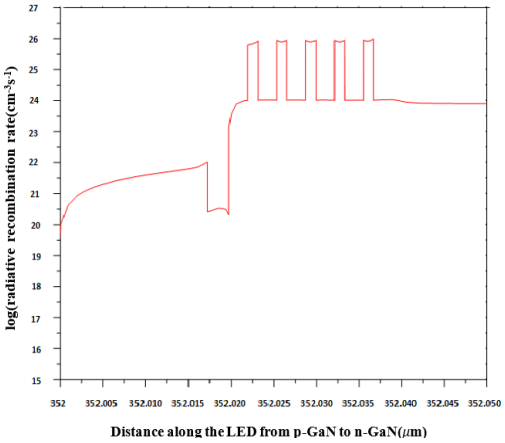

Al-0.2

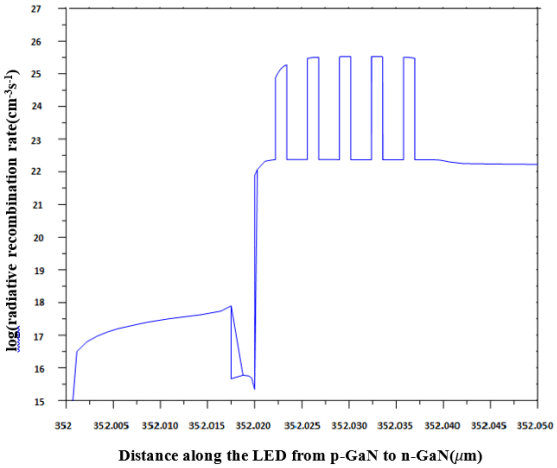

Fig 5.6 Rates of radiative recombination in the LED with different Al composition.

The carrier concentration profiles offer valuable insights into the behavior of electrons and holes within the simulated LED structure.

As illustrated in Figure 5.4, electrons are highly concentrated within the quantum well, indicating strong confinement in the InGaN active layer. This is largely due to the favorable conduction band alignment, which enables efficient electron injection from the n-type region. The resulting high electron density in the active zone suggests optimal carrier transport and accumulation.

Similarly, Figure 5.5 depicts the hole concentration profile, which also peaks within the same quantum well. Despite the inherently lower mobility of holes in GaN-based materials, the simulation results indicate that a sufficient number of holes reach the active region. This presence is essential for radiative recombination, as both carrier types must overlap spatially.

Further confirmation is provided by Figure 5.6, which shows the radiative recombination rate. A distinct peak in this region reflects effective recombination of electrons and holes precisely within the InGaN layer, reinforcing the success of the structure in promoting light emission. This implies that the majority of carriers contribute directly to photon generation, a critical factor in achieving high-efficiency\operation.

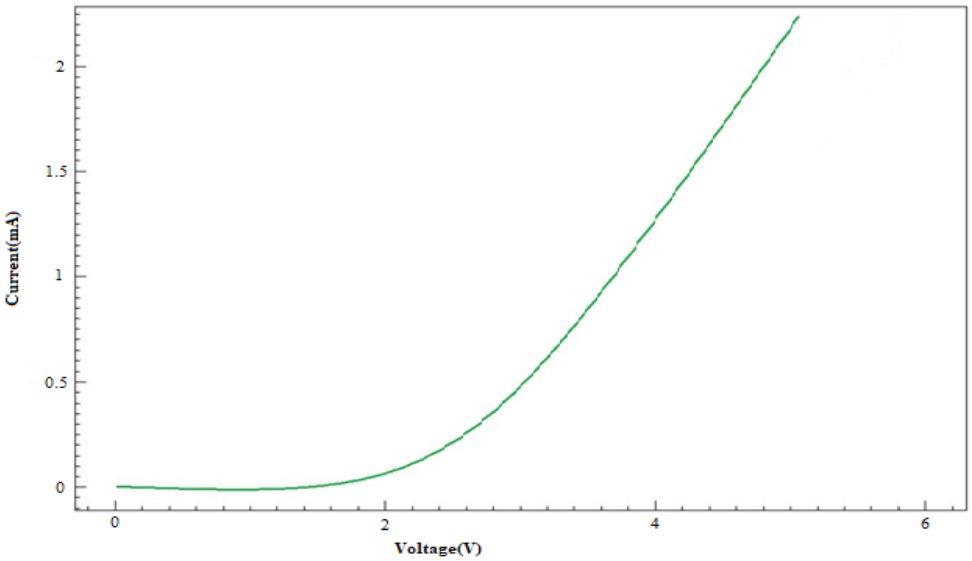

Fig 5.7 I-V curve

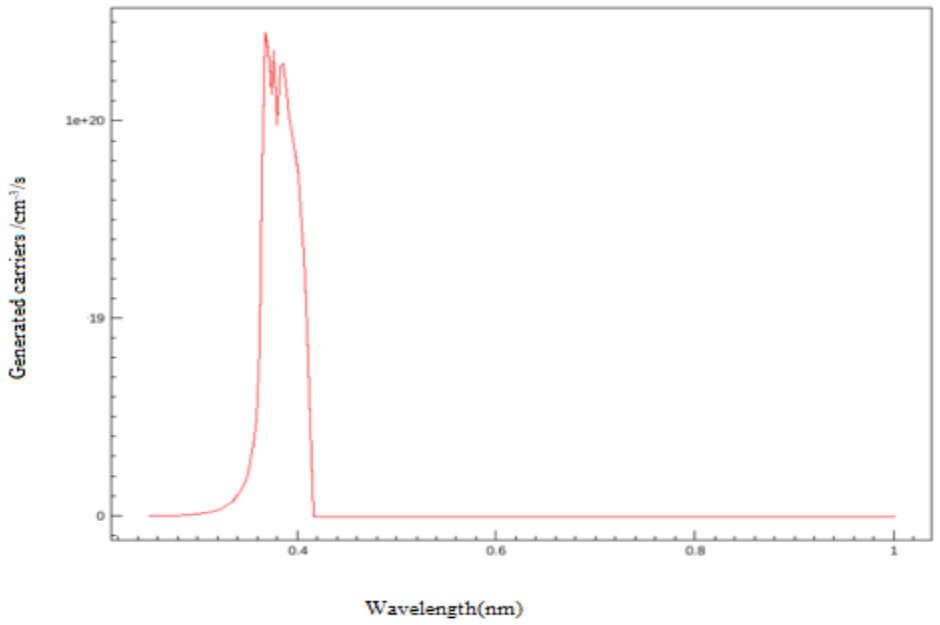

Fig 5.8 Optical generation of electron-hole pairs

The optical emission characteristics of the $In_{0.04}Ga_{0.96}N$/GaN multiple quantum well (MQW) LED were evaluated through ray tracing simulations using Sentaurus TCAD. Figure 5.8 presents the photon carrier density as a function of wavelength, highlighting the spontaneous emission behavior within the active region.

A distinct emission peak between 370 nm and 410 nm is observed, which falls in the near-ultraviolet to blue spectral region. This confirms that radiative recombination is taking place efficiently within the quantum wells and aligns well with the targeted wavelength for this composition of Indium (x = composit). Moreover, the narrow spectral width and the absence of significant emissions outside this range suggest good spectral selectivity and strong quantum confinement in the designed LED structure.

5.4 LED Characterization

The GaN-based LED developed for UV-blue emission was thoroughly characterized using advanced TCAD simulations. The analysis included an investigation of its electrical performance, carrier behavior, and optical activity. These simulations offer valuable insight into how the device performs under forward bias conditions, particularly in terms of current flow, carrier localization within the structure, and the strength and location of radiative recombination—all of which are critical for efficient light emission.

5.4.1 Electrical Characterization (I-V Analysis)

The electrical characteristics were examined by simulating the I–V response of the LED under forward bias. A clear and sharp rise in current was observed when the applied voltage exceeded approximately 2.8 V, marking the turn-on voltage of the device. This response indicates proper diode behavior, signifying effective carrier injection across the junction. The device's structure, based on a forward-biased p–i–n GaN configuration, demonstrates that both ohmic contacts and the active region have been successfully formed. This behavior confirms the electrical integrity of the device and its potential for practical optoelectronic applications.

5.4.2 Carrier Distribution

In terms of carrier distribution, the simulation revealed that electrons are predominantly confined within the InGaN multiple quantum wells due to a favorable conduction band offset. This ensures that a high concentration of electrons remains in the active region where light emission occurs. Although hole mobility in GaN is relatively low, the use of magnesium doping and an electron-blocking layer (EBL) successfully directs holes into the quantum well region, enabling effective recombination. It was also found that the aluminum composition in the EBL plays a significant role in determining performance. An Al content of around 10–15% helps block electron overflow while still permitting sufficient hole injection, thereby enhancing overall carrier confinement and recombination efficiency.

5.4.3 Radiative and Non-Radiative Recombination Including Efficiency

Extensive TCAD simulations were used to assess the electrical and optical performance of the GaN-based LED structure. Understanding how well the device transforms electrical input into light—a process that is largely dictated by the interaction between radiative and non-radiative recombination processes inside the active region—was one of the study's main goals. Effective carrier confinement and overlap were confirmed by the discovery that the main mechanism in the multiple quantum well (MQW) area was radiative recombination, in which electrons and holes recombine to generate photons. High internal quantum efficiency (IQE) can be directly determined by this. The internal quantum

efficiency was computed as the ratio of radiative recombination rate to total recombination rate, which incorporates contributions from both radiative and non-radiative routes, in order to further evaluate device efficiency.

To measure performance losses, non-radiative processes were also examined, particularly Shockley–Read–Hall (SRH) recombination and Auger recombination. The quality of material development and the efficacy of doping and layer engineering are highlighted by the low amount of SRH recombination, also known as "dark recombination," which is caused by trap states and crystal defects. In order to assess efficiency droop at large currents, the simulation took into account Auger recombination, which becomes important at high carrier concentrations. By increasing carrier confinement in the MQWs, the improved electron blocking layer (EBL) significantly reduced electron leakage and enhanced radiative recombination. With its high simulated IQE, low dark current losses, and negligible efficiency deterioration at higher bias levels, the device demonstrated significant optical output in the UV-blue spectrum overall, making it a viable option for energy-efficient underwater optical communication systems.

6

CONCLUSION & FUTURE SCOPE

Chapter 6

Conclusion

This project successfully demonstrates the design and simulation of Group-III nitride-based UV-blue LEDs using Multi-quantum well architectures in GaN/GaN, aimed at underwater optical communication. By tuning the indium composition and optimizing the layer dimensions, we achieved emission in the 370–410 nm range, which is ideal for low-loss transmission in water. The use of simulation tools like Synopsys Sentaurus TCAD allowed us to analyze carrier distribution, recombination behavior, and optical efficiency under different structural conditions. The study also highlighted the impact of polarization fields and how design strategies—such as using electron blocking layers—can improve performance. Overall, this work lays the groundwork for developing compact, efficient, and high-speed light sources that could be crucial for underwater wireless communication and related optoelectronic applications.

Future Scope

The development of Group-III nitride-based UV-blue LEDs offers immense potential for advancing underwater wireless optical communication (UWOC) systems. While the current work lays a solid foundation through simulation and design, future progress can focus on experimental fabrication and real-time deployment of the proposed LED structure. Implementing these devices in underwater environments will provide valuable insights into their performance under varying pressure, temperature, and turbidity conditions. Further, transitioning from polar to semi-polar or non-polar GaN substrates can help suppress polarization fields, thereby enhancing internal quantum efficiency. Light extraction efficiency (LEE) can also be improved through surface engineering techniques such as photonic crystals or roughened interfaces. Additionally, thermal management strategies must be explored to ensure long-term stability at higher power densities. Co-designing matching photodetectors for the same wavelength range will enable the development of efficient optical transceivers. Beyond communication, the optimized UV-blue LEDs can be repurposed for marine biological sensing, environmental monitoring, or medical diagnostics. Overall, this work opens up multiple avenues for advancing compact,

high-speed, and energy-efficient optoelectronic systems for both underwater and terrestrial applications.

REFERENCES:

[1] Gu H, Hu Y, Zhang Y, and Zou Y. A review of wide bandgap semiconductor nanowire-based ultraviolet detectors. Basel sensors. doi: 10.3390/s18072072; 2018 Jun 28;18(7):2072. PMCID: PMC6068994; PMID: 29958452.

[2] "Candelaclass highbrightness in-gan/algan double heterostructure blue light emitting diodes," Applied Physics Letters, volume. 64, pp. 1687, 1994, by Shuji Nakamura, Takashi Mukai, and Masayuki Senoh.

[3] Fan & Gila, Brent & Norton, David & Abernathy, Jenshan & Pearton, Stepehn, Byoung & Hung-Ta, Wang & Tien, Li-Chia & Ren, and Cammy & Lin. (2006). Thin film gas sensors and semiconductor nanorods with a wide bandgap. 6. 10.3390/s6060643 Sensors.

[4] "Photonic crystals improve led efficiency," by Daniel L. Barton and Arthur J. Fischer, The International Society for Optical Engineering, 2006.

[5] In "Improved characteristics of ingan multiple-quantum-well light-emitting diode by gan/algan distributed bragg reflector grown on sapphire," N. Nakada, M. Nakaji, H. Ishikawa, T. Egawa, and M. Umeno write in Applied Physics Letters, vol. 76, pp. 1804, 2000.

[6] "Low-resistivity and transparent indium-oxide-doped zno ohmic contact to p-type gan," Applied Physics Letters, vol. 85, no. 25, 2004; Jae-Hong Lim, Dae-Kue Hwang, Hyun-Sik Kim, Jin-Yong Oh, Jin-Ho Yang, R. Nava-mathavan, and Seong-Ju Parka.

[7] "Fundamentals of photonics," by Baaha E.A. Saleh and Malvin Carl Teich, 1991.

[8] Gerhard Klimeck Alejandra J. Saumitra Magana "Carrier statistics lab learning materials," by Raj Mehrotra and Dragica Vasileska, nano, 20010.

[9] Group-III-nitride and halide-perovskite semiconductor gain media for enhanced spontaneous emission and lasing applications [9] Khee Ng et al. 2021 Appl. Phys. 54 143001 Phys. D

[10] In N- and Ga-face AlGaN/GaN heterostructures, Kang, Byoung-Hung-Ta, and Wang "Two-dimensional electron gases induced by spontaneous and piezoelectric polarization charges" vol. 6, doi: 10.1063/1.369664.

[11] Keller, Stacia "Recent developments in (0001) N-polar group-III nitride metal-organic chemical vapor deposition" Technol. Semicond. Sci. 2014 29 113001 29/11/113001 https://iopscience.iop.org/0268-1242

[12] Farsane Tabataba-Vakili. (2020). III-nitrides on silicon: an ultraviolet-to-near-infrared integrated photonics platform.

[13] "Coherent (visible) light emission from ga(as1-xpx) junctions," by Nick Holonyak and S. F. Bevacqua, Applied Physics Letters, vol. 1, no. 4, pp. 82–83, 1962.

[14] "Efficiency of gaas1−xpx electroluminescent diodes," Solid State Electronics, vol. 10, no. 9, 1967, by H.P. Maruska and J.I. Pankove.

[15] Photoluminescence of mg-doped p-type gan and electroluminescence of gan p-n junction led by I. Akasaki, H. Amano, M. Kito, and K. Hiramatsu, Journal of Lumminescence, vol. 48, pp. 666–670, 1991

[16] "The preparation and properties of vapor deposited single crystalline gan," Applied Physics Letters, vol. 15, no. 10, 1969, by H.P. Maruska and J.J. Tietjen.

[17] Miller "Gan electroluminescent leds," RCA review, vol. 32, no. 3, pages. 383, 1971; Ea Pankove Ji and BERKEYHE.JE.

[18] "Preparation of mg-doped gan diodes exhibiting violet electroluminescence," Materials Research Bulletin, vol. 7, no. 8, pp. 777–781, 1972, Rhines W. C., Maruska H. P., and Stevenson D. A.

[19] K. Hiramatsu "P-type conduction in mg-doped gan treated with low-energy electron beam irradiation," vol. 28, pp. L2112–L2114, 1989, H. Amano, M. Kito, and I. Akasaki.

[20] "High-brightness ingan blue, green, and yellow light-emitting diodes with quantum well structures," Journal of Applied Physics, vol. 34, pp. 797–799, 1995; Nakamura S, Senoh M, Iwasa N, and Nagahama S.

[21] June O. Song, Jun-Seok Ha, and Tae-Yeon Seong, "Ohmic-contact technology for gan-based light-emitting diodes: Role of p-type contact," IEEE Transactions on Electronic Devices, vol. 57, no. 1, 2010.

[22] Applied Physical Letters, vol. 68, pp. 1403, 1996; M. Koike, S. Yamasaki, S. Nagai, N. Koide, S. Asami, H. Amano, and I. Akasaki, "High-quality gainn/gan multiple quantum wells."

[23] "Light extraction from optically pumped light-emitting diode by thin-slab photonic crystals," Applied Physics Letters, vol. 75, pp. 8, 1999, by M. Boroditsky, T. F. Krauss, R. Coccioli, R. Vrijen, R. Bhat, and E. Yablonovitch.

[24] Kobayashia, S. Yamasakib, S. Nagaib, S. Umezakib, J. Masanori Murakam, M. Koikeb Applied Surface Science, vol. 117, no. 2, pp. 373–379, 1997; Yasuo Koide, H. Ishikawaa, "Dependence of electrical properties on work functions of metals contacting to p-type gan."

[25] "A study of transparent indium tin oxide (ito) contact to p-gan," Thin Solid Films, pp. 398–399, 2001, by D.W. Kim, Y.J. Sung, J.W. Park, and G.Y. Yeom.

[26] Mansun Chan Theodore I. Kammins and Richard S. Muller, "Device electronics for integrated circuits," 2002